IS-4758
UC-90h

Alloy Evaluation for Fossil Fuel Process Plants (Liquefaction)

Annual Report for

Period

1 October, 1979 through 30 September, 1980

C. M. Woods and T. E. Scott

AMES LABORATORY

Iowa State University

Ames, Iowa 50011

October 15, 1980

PREPARED FOR THE UNITED STATES DEPARTMENT OF ENERGY
UNDER CONTRACT NO. W-7405-Eng-82, & NUMBER WPAS-AA-60-03-01

fcq

DISCLAIMER

Printed in the United States of America

Available from
National Technical Information Service
U.S. Department of Commerce
5265 Port Royal Road
Springfield, VA 22161

Price:

Microfiche	$3.50
Fullsize	9.50

FOREWORD

This report covers work performed during the period 1 October, 1979 through 30 September, 1980. The work was funded by the Office of Advanced Research and Technology under the Assistant Secretary for Fossil Energy and was monitored by R. A. Bradley, Manager of Fossil Energy Materials Projects at Oak Ridge National Laboratory. The report was prepared by Charles M. Woods and T. E. Scott of the Mechanical Properties Section in the Metallurgy and Ceramics Division at the DOE-Ames Laboratory, Ames, Iowa.

The work was performed under the direction of Dr. Scott as principal investigator assisted by: C. M. Woods, S. Shei, C. V. Owen and L. K. Reed.

ABSTRACT

An electropotential measurement system for monitoring crack growth in fatigue specimens was constructed. An electrically isolated loading cage including specimen grips and universal joint was designed and built for use in crack growth studies with our five inch I.D. autoclave dynamic test facility. A potential drop vs. crack growth calibration curve for dynamically loaded compact tension specimens (CTS) of A387-74A-Gr.22-Cl.2 steel was established. Fatigue crack growth rates (da/dN) were determined for a wide variation of stress intensity range values (ΔK). Testing was done in moist air ($\sim$30% RH) at ambient temperature and pressure and in hydrogen gas at ambient temperature and various pressures. Near-threshold to rapid crack growth stages were examined. Baseline J_{IC} data were determined in 800°F argon gas at ambient pressure. A K_{IC} value was extracted from the

J_{IC} data. Bolt-loaded compact tension specimens (BLCTS) were loaded and exposed to a coal slurry environment. The test was aborted after ∿200 hours due to a rupture disk failure.

The average thermal expansion coefficient for Carpenter 883 (H-13, the bolt material for bolt-loaded compact tension specimens) was determined for the temperature range 72°F to 800°F. The thermal stability, as a function of time, was determined at 800°F. The average thermal expansion coefficients for both A387-74A-Gr.22-Cl.2 steel and 316 stainless steel were determined for the 72°F to 1000°F temperature range. Thermal stability of A387 at 1000°F was monitored for a period of 250 hours. Ring-sample relaxation tests were run in argon at 950 and 1000°F for 350 and 250 hours respectively. Sample stress vs. exposure time was obtained. Load vs. deflection calibration curves were determined for 316 stainless steel loading rings at 76, 200, 400, 600, 820 and 1000°F. Ring compliance constants (K_r) were determined and plotted vs. temperature. Compliance curves for bolt-loaded compact tension specimens were determined at room temperature and 800°F for three different crack lengths (a).

Smooth-bar and notched-bar tensile specimens of A387-74A-Gr.22-Cl.2 steel were exposed to 4000 psig H_2 gas at 1000°F for 168, 250 and 500 hours. Samples were exposed in the unstressed, stressed, and prestrained conditions. Tensile tests were made in air at room temperature at the end of each exposure. Metallographic examinations were made of fracture surfaces as well as other exposed specimens not subjected to the tensile testing. The exposed material exhibited a marked reduction in notch ductility as well as a small reduction in notch tensile strength. The smooth-bar samples showed no significant changes in mechanical properties even after 500 hours

of exposure. SEM examinations revealed the presence of small bubbles that formed mostly on or near grain boundaries and in the vicinity of second phase particles. Specimens cleaved at liquid nitrogen temperature exhibited bubbles on the fracture surface. The same tests as above were carried out on notched-bar specimens exposed to 4000 psig H_2 gas at 950°F for 350 hours. Some evidence of bubble formation was seen in the vicinity of the notch of stressed notched-bar samples as well as near second phase particles. Bubble formation was noted near second phase particles in prestrained samples but was not seen in any of the unstressed specimens. The formation of bubbles was very scarce and extensive searching had to be done to see them. The exposed material showed no marked changes in room temperature mechanical properties with the exception of the prestrained samples. The prestrained samples showed a slight decrease in notch ductility.

Corrosion specimens of A387-74A-Gr.22-Cl.2 steel were exposed to a coal slurry environment at 800°F, 4000 psig total pressure for 24, 48, 72 and 240 hours. Corrosion scale growth rates and micrographs of the scale region are presented.

Random samples of the Kentucky bituminous and coal derived oil used for coal slurry exposures were analyzed for total sulfur and chlorine content.

Phase stability diagrams for Fe, Cr, Mo, and Mn in H_2S/H_2-O, H_2S/H_2-C, and C-O environments were derived and are presented.

OBJECTIVE AND SCOPE

The objective of this program is to evaluate the mechanical properties of liquefaction process plant "dissolver" vessel materials in a "dissolver" vessel environment including coal slurry and pressurized hydrogen gas at temperatures up to 800°F. Originally, the intent was to test at 900°F but we soon learned that above 850°F (455°C) gasification is ignited giving coke and methane. Consequently, all runs originally indicated as 900°F will be run at 800°F to assure there are no excursions above the critical gasification ignition temperature.

Specifically, the degradation of notched-bar and smooth-bar tensile samples of 2 1/4 Cr-1 Mo will be monitored as a function of exposure time and stress in the "dissolver" vessel environment. Compact tension specimens will be used to monitor the degradation of fracture properties in the "dissolver" vessel environment.

Notched-bar tensile specimens will be used to evaluate the behavior of 2 1/4 Cr-1 Mo steel in pure hydrogen gas at various temperatures and pressures. The objective is to determine the Nelson curve.

PROGRESS SUMMARY

I. Fracture Mechanics Tests

A. Procedure and Results:

An electropotential measurement system for monitoring crack growth in dynamically loaded compact tension specimens was constructed. The system incorporates a Norbatron DCR 60-13A constant current power supply with a Keithley Model 174 digital multimeter interfaced to a Keithley Model 750

printer (Fig. 1). Excitation current to the specimen is switched on and off by means of a battery driven relay. This enables potential drop measurements across the crack to be made at preset intervals with the excitation current both on and off. The difference between the two measurements is taken as the true potential drop across the crack. This allows elimination of thermal potentials and other transients. The relay is activated by a Darlington transistor switching circuit that has been appropriately interfaced with a switching circuit in the printer. The printer circuit switches from lo to hi and back to lo again as the printer cycles through a double print phase. The printer can be cycled every 2 to 120 seconds depending on the time increment desired for making the potential drop measurement. The excitation current is 5 amps. The sensitivity of the multimeter is ± 0.1 μV which corresponds to a resolution of crack growth of $\sim \pm 0.5$ mils. The system stability has been determined to be better than ± 0.2 μV per day after warm-up which gives a resolution of better than ± 1.0 mil of crack growth increment. Calibration of the crack growth measurement system will be subsequently described.

Compact tension specimens (CTS) (Fig. 2) were prepared from a 0.75 inch thick hot rolled plate of A387-74A-Gr.22-Cl.2 steel. The starter notch was machined perpendicular to the rolling direction (ASTM specification E-399, L-T type specimen). The surface of the specimens was mechanically polished to 600 grit. Two specimens were precracked to a total crack length, 'a' (as measured from the load line to the tip of the precrack), of 0.85 and 1.33 inches respectively using an MTS-series 810 electrohydraulic test system. The precracking was done in load control. The frequency was 20 Hz. and the loading was sinusoidal in a tension-tension mode with the

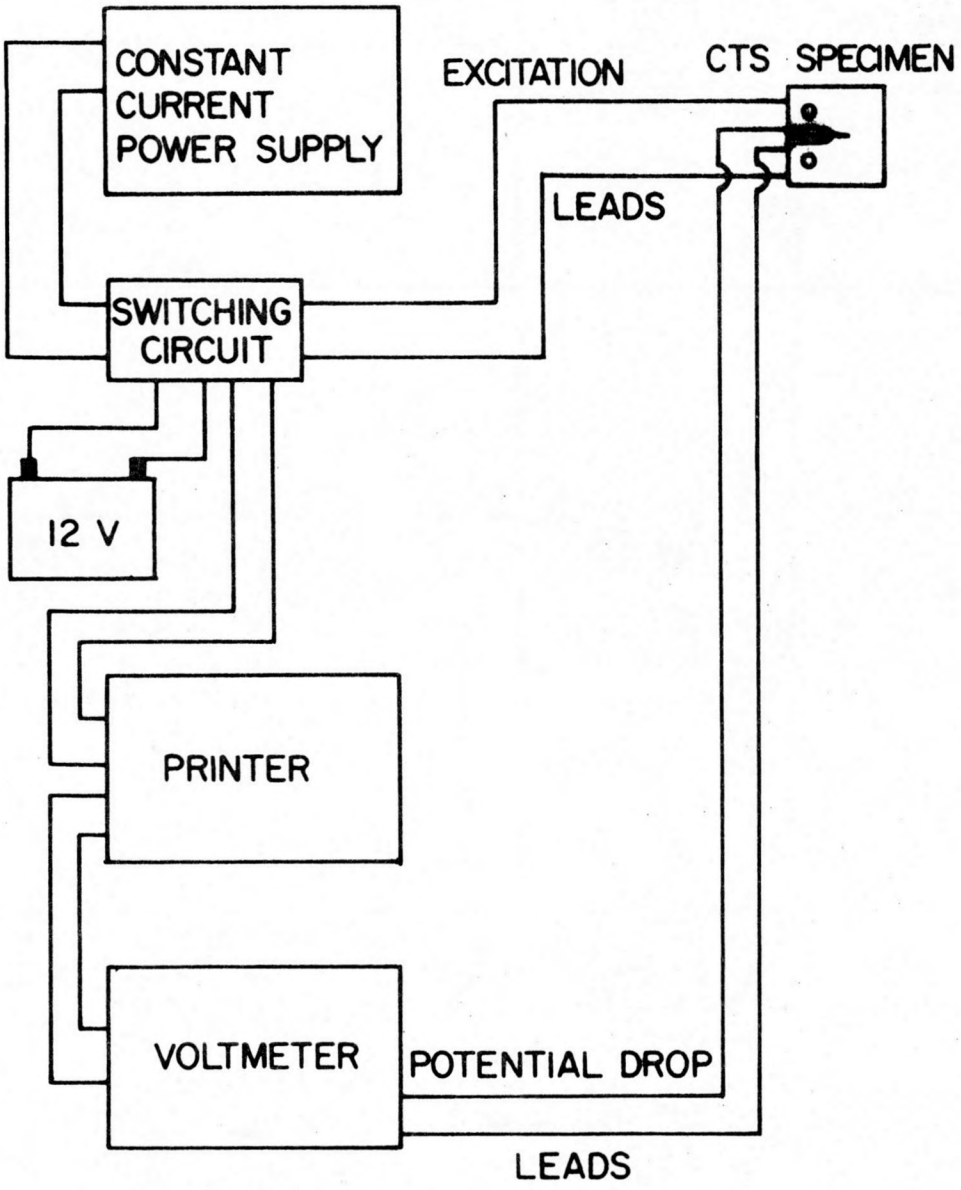

Fig. 1: Block Diagram of Electropotential Measurement System.

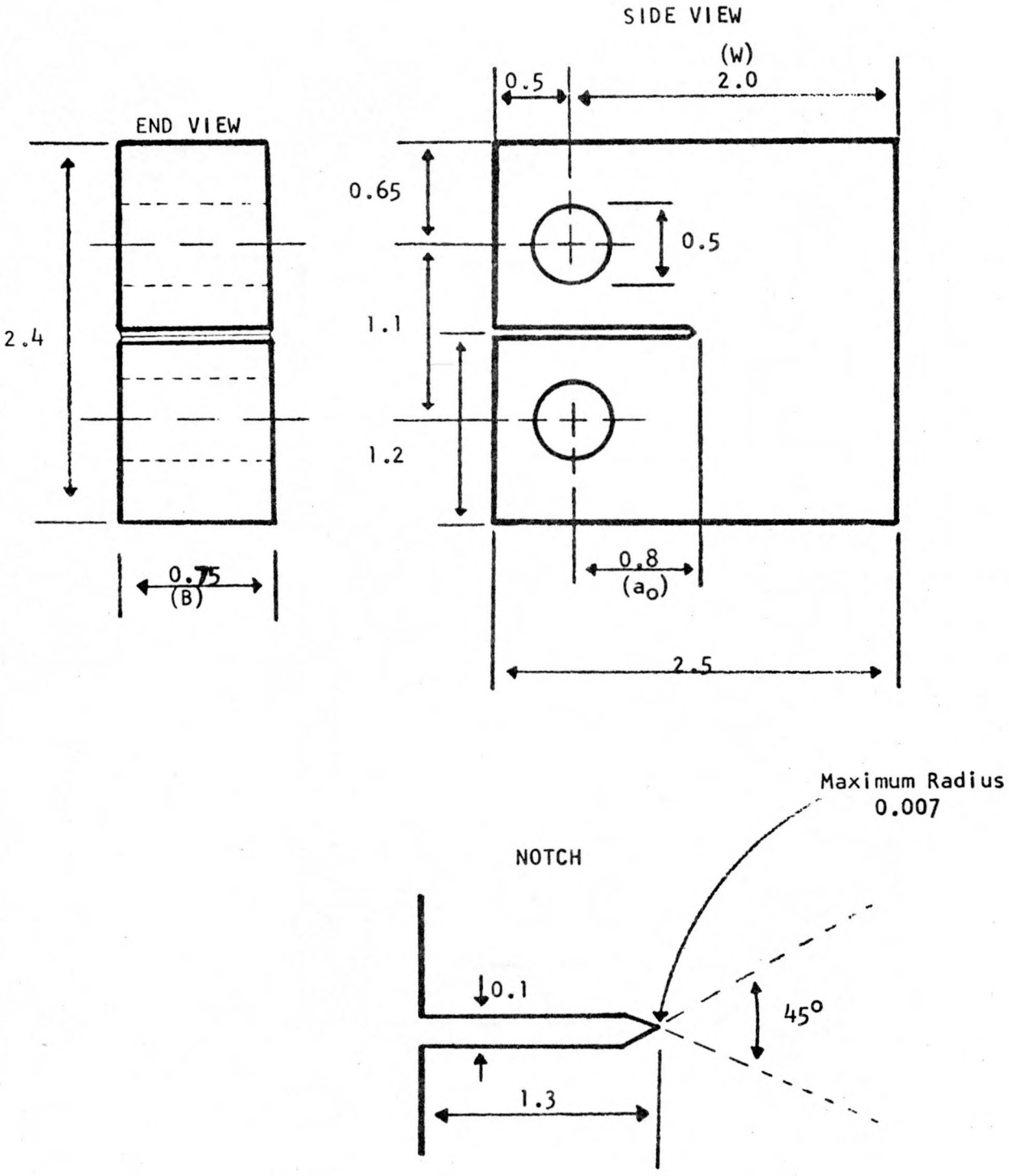

Fig. 2: 2 1/4 Cr-1 Mo Compact Tension Specimen. All dimensions are in inches.

minimum load controlled at 10% of the maximum load. The maximum load criterion was derived as shown in the following analysis. The ASTM E-399 fatigue precracking procedure requires that —

$$K_{f\ max} \leq 0.002\ E\sqrt{in}\ .$$

However for the CTS, K_f is given by —

$$K_f = (P/B\sqrt{a})\ f(\frac{a}{w})\ .$$

Rewriting the preceding equation in terms of maximum load gives —

$$P_{max} = \frac{K_{f\ max}(B\sqrt{a})}{f(a/w)}\ .$$

Inserting the ASTM E-399 condition for $K_{f\ max}$ as given above leads to the maximum load criterion —

$$P_{max} \leq 0.002\ E\ (\frac{B\sqrt{a}}{f(a/w)})\ ,$$

where, $K_{f\ max}$ = maximum stress intensity of the fatigue cycle

E = Young's modulus

P = load

B = specimen thickness

a = crack length

f(a/w) = measure of the compliance of the specimen.

P_{max}, for each of the two specimens, was chosen as the greatest value of load that satisfied the inequality at 'a' equal to 0.85 and 1.33 inches respectively.

Excitation current was applied by attaching copper leads to two threaded holes positioned one on each side of the notch at the notch end of the specimen (Fig. 3). The holes were drilled and tapped at the center of the thickness dimension (B) at 0.295 inches in from the outer edge of the specimen. Potential drop measurements were made by attaching leads to two threaded holes, one on each side of the notch, positioned at the center of the thickness dimension and 0.197 inches out from the notch center (Fig. 3).

Each specimen was cycled in load control at 20 Hz. for ΔK values never exceeding 40 ksi $\sqrt{in}$. ΔK was calculated as follows:

$$\Delta K = (P_{max} - P_{min}) \frac{f(a/w)}{B\sqrt{a}}$$

where, P_{max} = maximum load of fatigue cycle

P_{min} = minimum load of fatigue cycle.

The load cycling was stopped after each 10 μV change ($\sim$3 μV for the second specimen) in the potential drop measurement and the crack size was measured on the surface of the sample. A plot of Va/Va_o vs. a/a_o is presented in Fig. 4 for both specimens. It is apparent that the curve is linear, reproducible and independent of initial crack length. The slope of the calibration curve is shown to be 0.861.

Fatigue crack growth rates (da/dN) were determined as a function of stress intensity range (ΔK) in moist ($\sim$30% RH) air at ambient temperature and pressure. A compact tension specimen was precracked to a total crack length of 0.85 inches using the procedure outlined above. The precracked specimen was then cycled at 20 Hz. in load control at a ΔK value of 10 ksi $\sqrt{in}$. The loading was sinusoidal with P_{min} controlled at 10% of

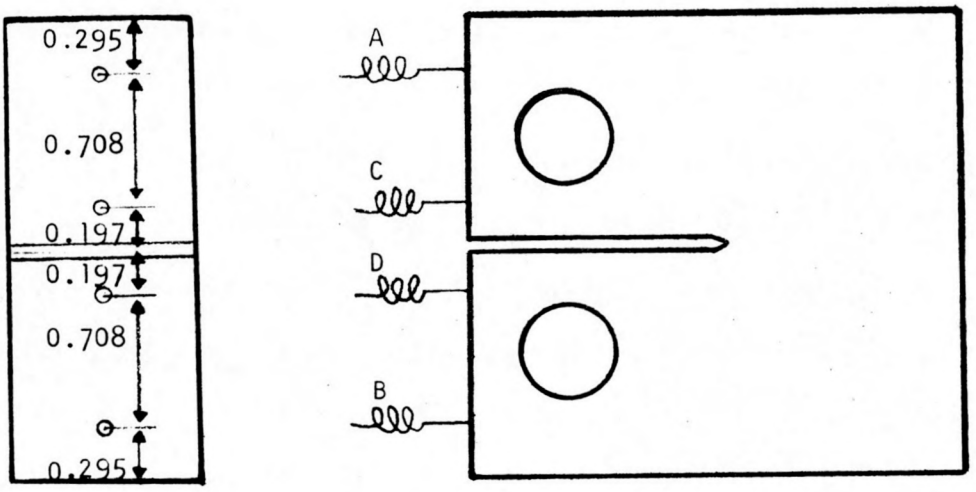

A & B - Excitation Leads

C & D - Potential Drop Leads

All dimensions in inches

Fig. 3: 2 1/4 Cr-1 Mo Compact Tension Specimen showing position of excitation and potential drop leads.

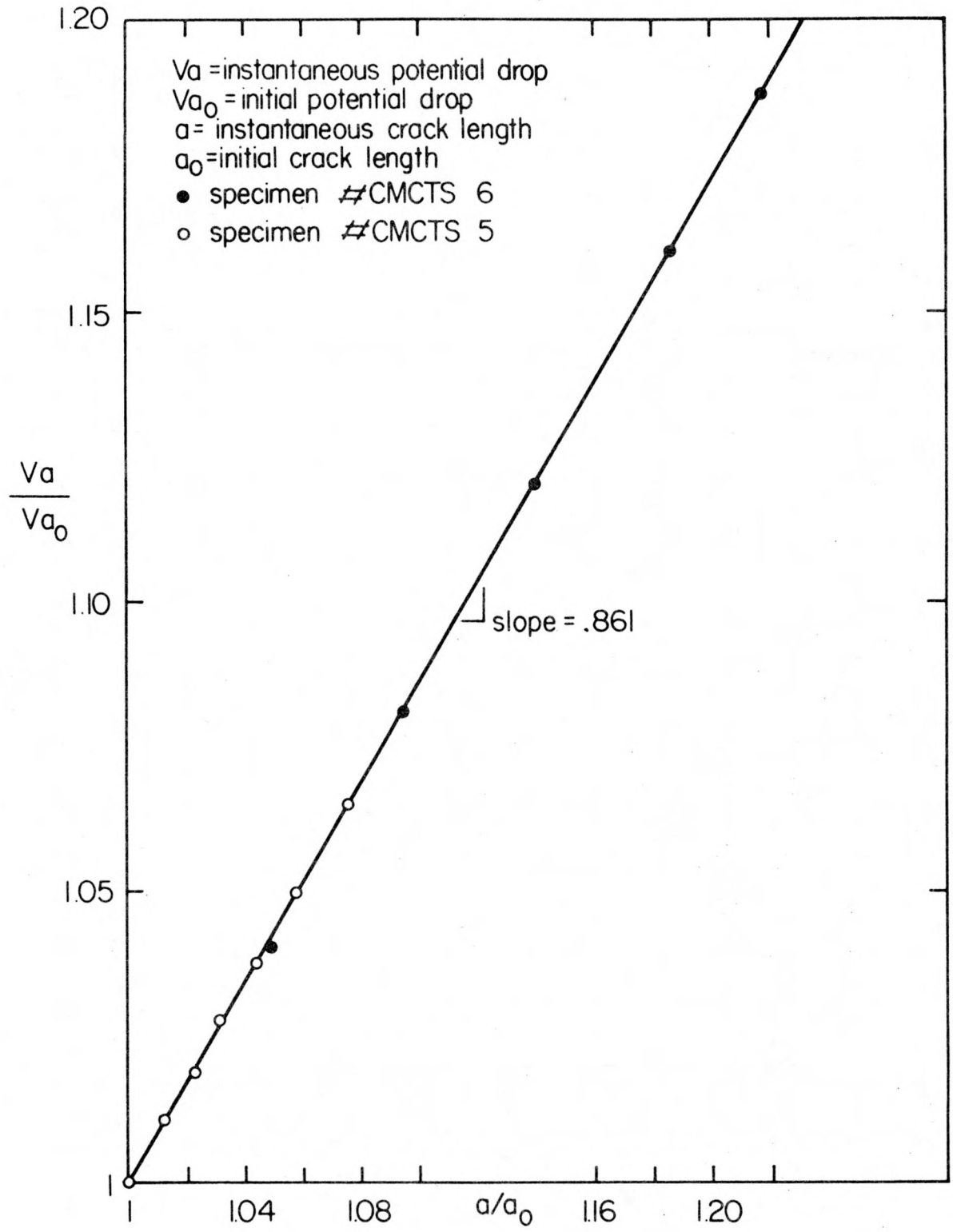

Fig. 4: Normalized potential drop vs. crack growth calibration curve for 2 1/4 Cr-1 Mo, .75T- Compact Tension Specimen.

P_{max} ($R=0.1=P_{min}/P_{max}$). The loading was carried out until the crack growth rate was detected to be uniform over moderate periods of time. This assured that the plasticity ahead of the crack due to the precracking procedure would not affect the determination of the stress intensity threshold (ΔK_{TH}). The stress intensity range was decreased in 10% increments until crack growth could not be detected in 2×10^5 cycles. Since the resolution of the crack growth measurement system is $\sim \pm 1$ mil, this corresponds to a crack growth rate of 5×10^{-9} in./cycle. This was termed the stress intensity threshold. ΔK_{TH} was determined to be 8.5 ksi $\sqrt{in}$ in moist air at ambient temperature and pressure. Fatigue crack growth rates were then determined for ΔK values ranging from threshold to $\sim$40 ksi $\sqrt{in}$. The results were plotted as log da/dN vs. log ΔK (Fig. 5).

The same test, as outlined above, was repeated in hydrogen gas at 15 psig and ambient temperature. ΔK_{TH} was lowered to 6.5 ksi $\sqrt{in}$ due to the presence of the hydrogen gas. Crack growth rates (da/dN) above ΔK values $\sim$10 ksi $\sqrt{in}$ were not appreciably affected by the presence of hydrogen gas at 15 psig (Fig. 5). The hydrogen pressure was increased to 1000 psig and the test repeated. Threshold values were not investigated due to system problems that have recently been corrected. Crack growth rates above ΔK values of $\sim$15 ksi $\sqrt{in}$ appear to be slightly accelerated due to the presence of 1000 psig H_2 gas (Fig. 5).

Four compact tension specimens (CTS) (Fig. 2) were prepared, as outlined above, from a 0.75 inch thick hot rolled plate of A387-74A-Gr.22-Cl.2 steel. The specimens were precracked, using the procedure outlined previously, to a total crack length, 'a' (as measured from the load line to the tip of the precrack), of 1.2 inches. Each specimen was then heated to 800°F

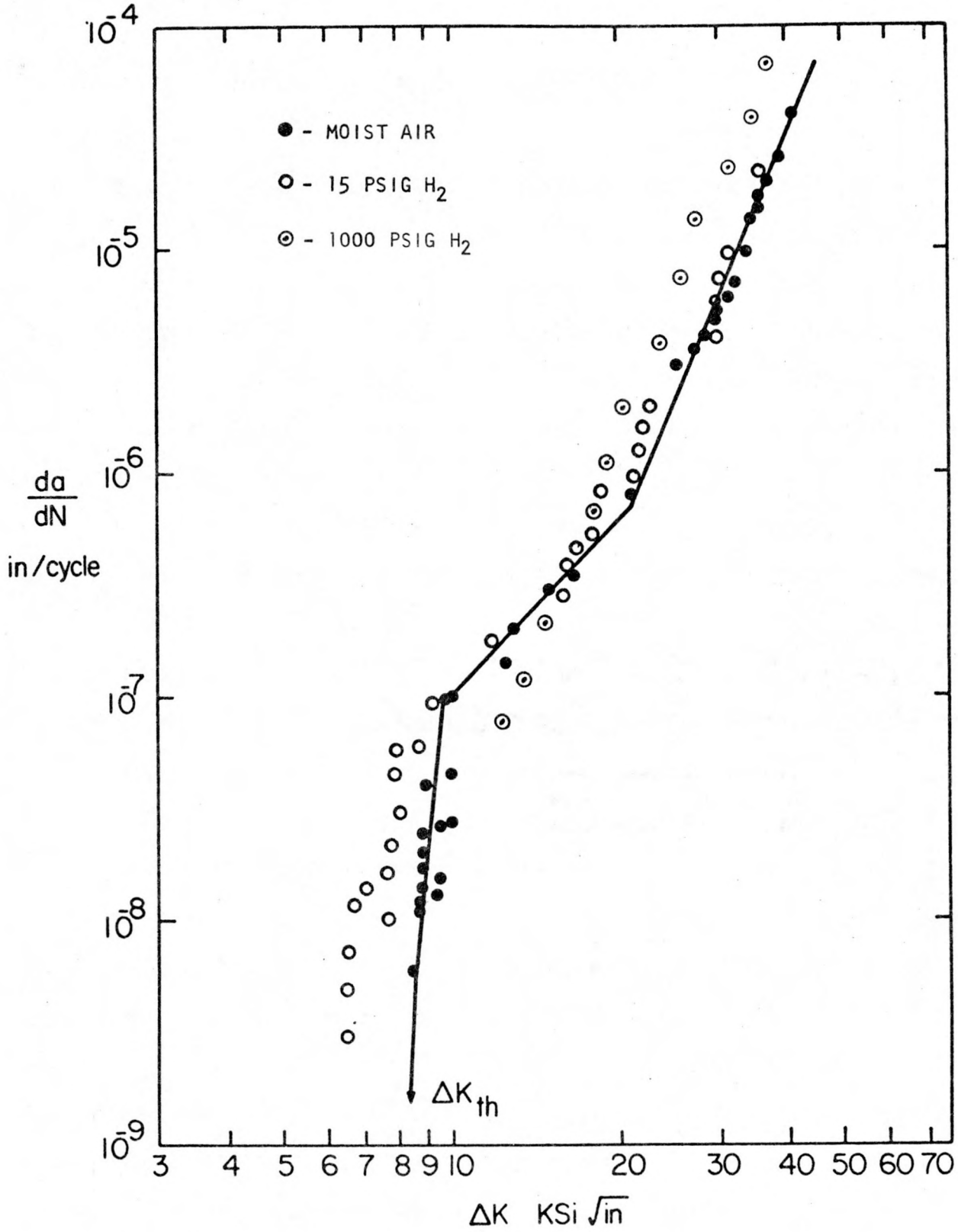

Fig. 5: Fatigue crack growth rate curves for 2 1/4 Cr-1 Mo steel at ambient temperature.

in argon and pulled to a predetermined value of J (determined by graphical integration of the area under the load vs. load-line displacement curve). The specimens were allowed to cool and were subsequently pulled apart at liquid nitrogen temperature. The amount of crack extension, 'Δa', that occurred from loading to various J values at 800°F was measured using a Gaertner traveling microscope. The value recorded was the point of maximum crack extension measured from the fatigue precrack. Each value of J was then plotted vs. its corresponding crack growth increment 'Δa'. A blunting line was then plotted and the intersection of the two curves was taken to be J_{IC}. The blunting line was defined as —

$$J = 2\,\sigma_{flow}\,\Delta a$$

where, $$\sigma_{flow} = \frac{\sigma_{YS} + \sigma_{UTS}}{2}\,.$$

K_{IC} was obtained from —

$$J_{IC} = G_{IC} = \frac{1-\nu^2}{E}\,K_{IC}^2$$

where, ν = Poisson's ratio

E = Young's modulus

K_{IC} = plane strain, static loading, critical stress intensity factor

$J_{IC}=G_{IC}$ = plane strain energy release rate per increment of crack growth.

J_{IC} was determined to be 1105 in-lbs/in^2 at 800°F in argon for bainitic A387-74A-Gr.22-Cl.2 steel. The value of K_{IC} that corresponds to this value of J_{IC} was computed as 184 ksi $\sqrt{in}$ (Table 1).

Two bolt-loaded compact tension specimens of A387-74A-Gr.22-Cl.2 steel

TABLE #1

J_{IC} TESTS

Material	Test Temp. (°F)	Environment	J_{IC} (in-lbs/in^2)	K_{IC} (ksi$\sqrt{in}$)
A387	800	Argon	1105	184

(Fig. 6) were prepared in the same way as the compact tension specimens previously described. Precracking was done in the same manner as mentioned above. The specimens were loaded at room temperature (via the bolt) to a predetermined value of K (stress intensity). The specimens were placed in a 304 stainless steel can containing coal slurry. One sample was immersed in the slurry and the other was suspended above the slurry. The coal slurry was a blend of 35 volume percent of -100 mesh Kentucky bituminous (Proximate Analysis, wt.pct.: Moisture, 6.1; Ash, 15.5; Volatile Matter, 36.3; Fixed Carbon, 42.1) and 65 volume percent solvent. The sulfur content of the coal was 5.53 wt.pct. The solvent was centrifuged Synthoil product (Ash free wt.pct.: Organic benzene insols, 3.3; asphaltenes, 32.3; Oils, 64.4) from PERC Run FB-61 made from the coal described above. The coal and solvent were graciously supplied by Paul M. Yavorsky of PERC. The slurry was prepared by mixing the fine coal in the solvent which, because of its high viscosity (161 SSF at 180°F) at room temperature, was preheated to 110°F. The can was placed in a pressure vessel, 1500 psig H_2 was pumped in and the system was equilibrated to 800°F, 4000 psig total pressure.

The K value at temperature was calculated in the following manner. The problem was treated as two elastic bodies in static equilibrium undergoing a temperature deviation from room temperature. The equilibrium notch-front-face (NFF) displacement (at 800°F) was calculated to be —

$$\Delta\ell_{NT} = \frac{(\ell_B - \ell_N + \alpha_B \ell_B \Delta T - \alpha_N \ell_N \Delta T) E_B A_B}{K_{NT}(\ell_B + \alpha_B \ell_B \Delta T) + E_B A_B}$$

where, $\Delta\ell_{NT}$ = notch-front-face displacement at T

ℓ_B = straining portion of the loading bolt, this is a function of the room temperature NFF displacement

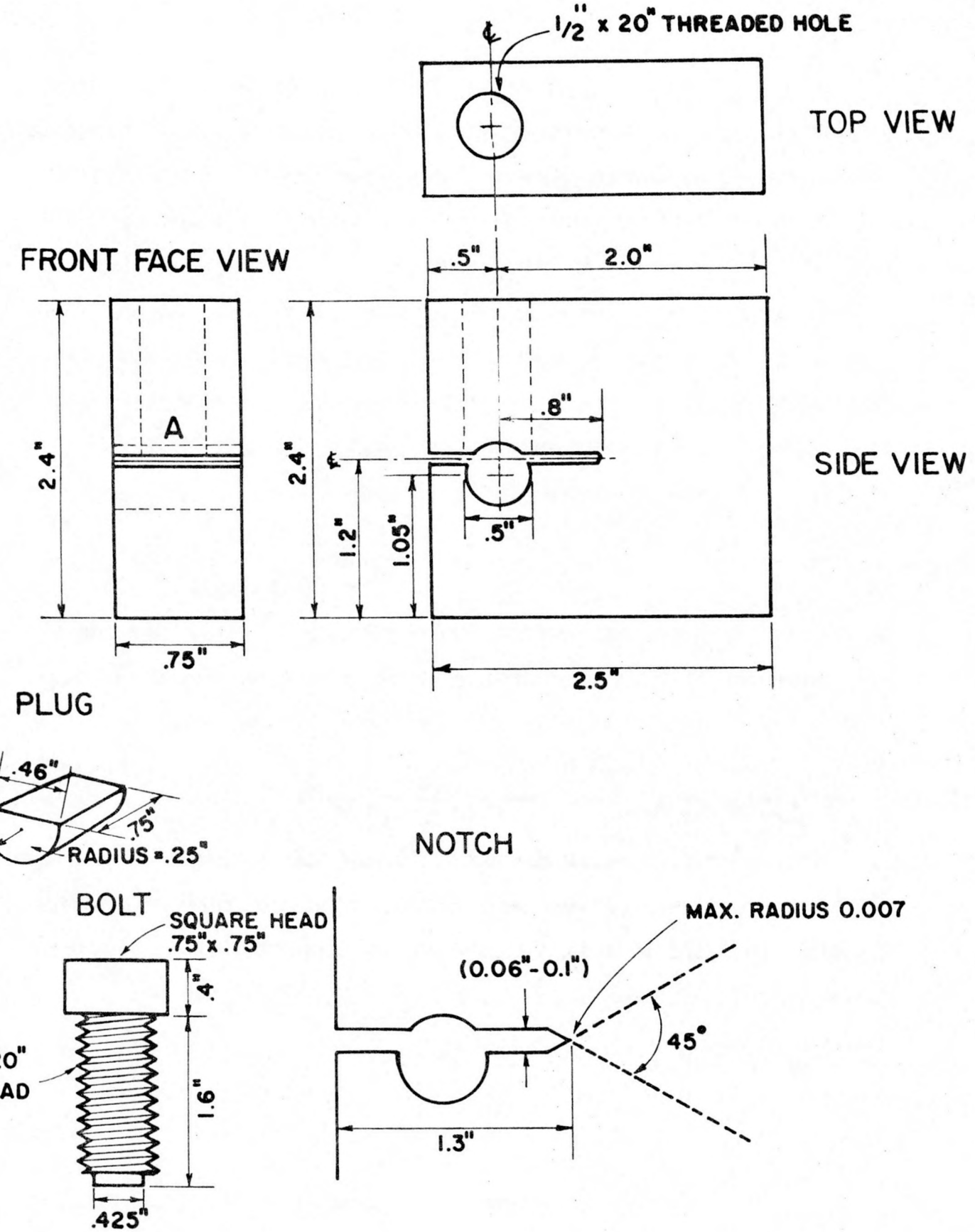

Fig. 6: 2 1/4 Cr-1 Mo Bolt-Loaded Compact Tension Specimen. All dimensions are in inches.

ℓ_N = notch gap length at room temperature

α_B = bolt material average thermal expansion coefficient for T range of interest

α_N = BLCTS material average thermal expansion coefficient for T range of interest

ΔT = temperature deviation (T - RmT)

E_B = Young's modulus of bolt material at T

A_B = bolt area at T

K_{NT} = BLCTS compliance coefficient at T (for initial crack length 'a').

The derivation of this equation is too lengthy to be presented here. The load exerted on the BLCTS by the bolt was calculated from —

$$P = K_{NT}\ \Delta\ell_{NT} \cdot$$

The stress intensity (K) was obtained from —

$$K = (P/B\sqrt{a})\ f(\frac{a}{w}) \ .$$

The two specimens were loaded to K values of 62.2 and 71.7 ksi$\sqrt{in}$ respectively at temperature (800°F) at the beginning of the test. The test was scheduled to last 350 hours. Unfortunately a rupture disk failure caused termination of the test at ∿200 hours. No crack extension was observed. The crack filled completely with a complex sulfur containing scale.

II. Thermal Expansion, Thermal Stability, and Compliance Tests

A. Procedure and Results:

Loading bolts for the 2 1/4 Cr-1 Mo bolt-loaded compact tension specimens (Fig. 6) were machined from a 1 1/4" rod of Carpenter 883 tool steel. The bolts, along with bolt rests (Fig. 6) and a thermal expansion specimen of the same material, were packed in gray iron chips and placed in a muffle furnace. The iron chips, bolts etc. were heated to 1875°F and held for 25 minutes. The parts were withdrawn from the furnace, removed from the gray iron chips and air cooled in still air to room temperature. The parts were then triple drawn (tempered) at 1025°F for two hours per draw with air cooling to room temperature between draws. The thermal expansion specimen was placed in a quartz thermal expansion rig and the average thermal expansion coefficient was determined for the temperature range 72°F to 800°F. The thermal expansion rig incorporates a capacitance gage having a resolution of 4×10^{-7} inches. The result is listed in Table 2. The specimen was then isothermally held at 800°F in argon and the specimen length monitored for 168 hours. The thermal stability is shown in Fig. 7.

Average thermal expansion coefficients for both A387-74A-Gr.22-Cl.2 steel and 316 stainless steel were determined, using the above mentioned rig, for the 72 to 1000°F temperature range. These values are listed in Table 2. The A387 was placed in the test rig and isothermally held in argon at 1000°F for 250 hours. The sample showed good stability as demonstrated in Fig. 8.

Ring-sample composite (Fig. 9) relaxation was monitored in argon at 1000°F for 250 hours. The ring was loaded in compression at room temperature in a compression cage on a TT-C Instron tensile test machine. The

TABLE #2

THERMAL EXPANSION DATA

Temperature Range (°F)	Material	Thermal Expansion Coefficient (μ in/in/°F)
72-500	A387	7.03±.04
72-800	A387	7.43±.02
72-900	A387	7.48±.02
72-1000	A387	7.53±.02
72-500	316 SS	9.54±.05
72-800	316 SS	9.87±.02
72-900	316 SS	9.93±.01
72-1000	316 SS	10.16±.01
72-800	883 (H-13)	7.07±.02

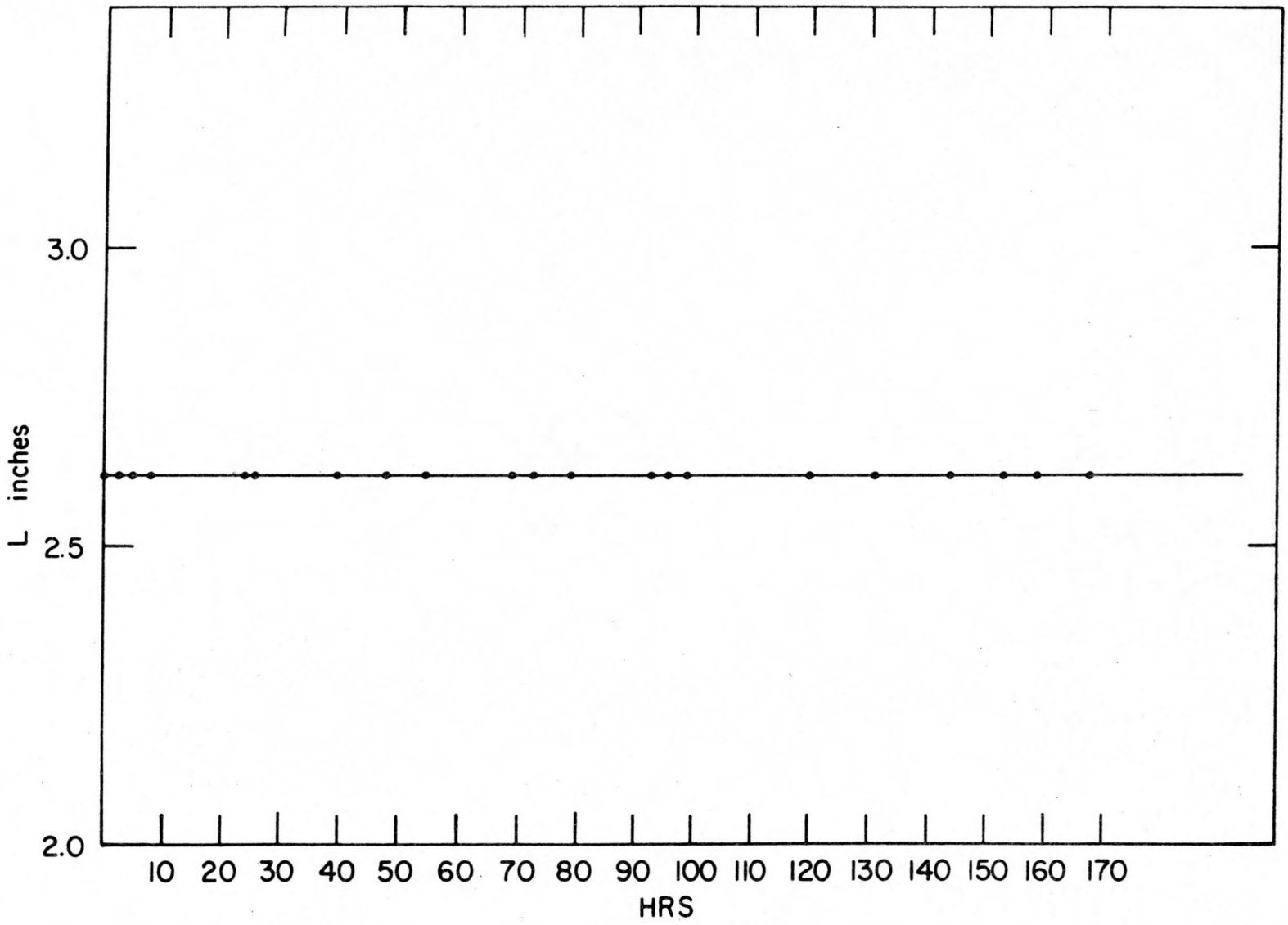

Fig. 7: Plot of thermal stability of Carpenter 883 (H-13) vs. time at 800°F in argon.

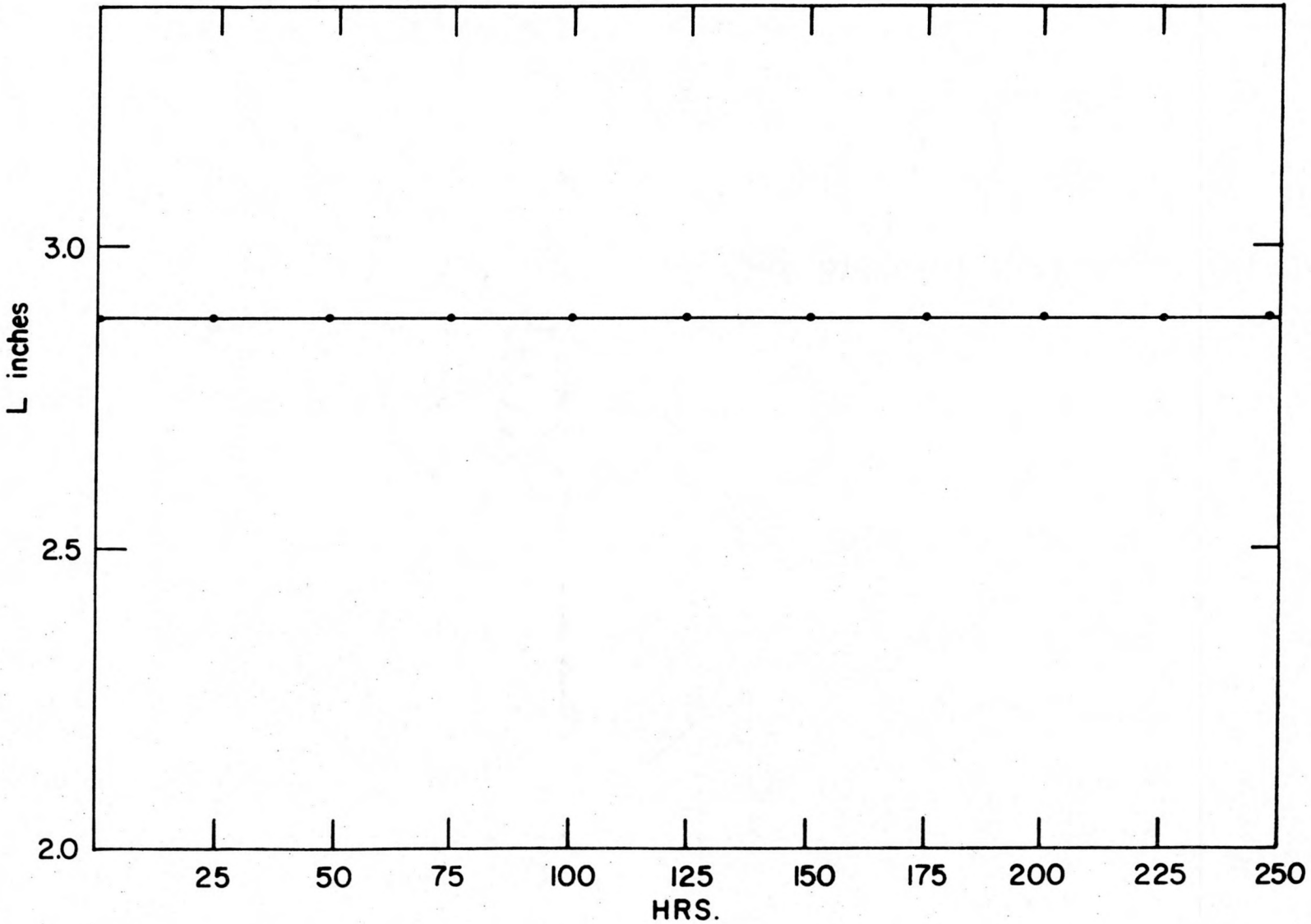

Fig. 8: Plot of thermal stability of A387 vs. time at 1000°F in argon.

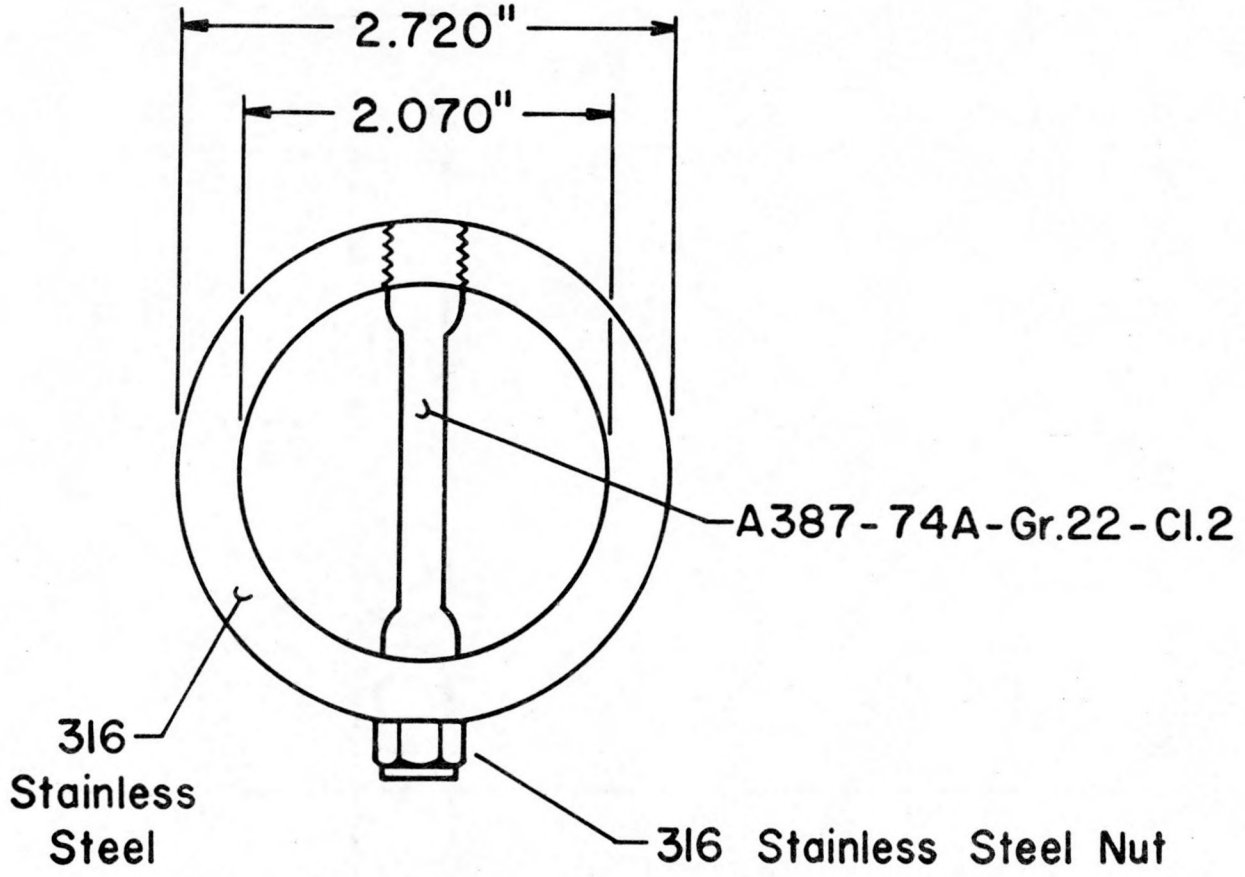

Fig. 9: Ring-Sample Composites for stressed exposures. Rings used in this study have O.D. = 2.554 inches.

load was transferred to a notched-bar tensile sample (Fig. 10) spanning the diameter of the pre-compressed ring by screwing the sample into the threaded section of the ring at one end and tightening a nut at the other end. The diameter of the ring was measured before and after loading and adjustments were made to achieve a predetermined value of ring deflection. The ring-sample composite was placed in a specially designed quartz thermal expansion rig and heated to 1000°F in argon gas. The ring-sample composite diameter was monitored as a function of time for 250 hours and is presented in Fig. 11. The stress in the sample during the course of the 250 hours is shown in Fig. 12. The stress was calculated as shown in the following analysis. The deflection of the ring at 1000°F was given by —

$$\Delta D_{1000} = D_{ring} - D_{comp.} \,, \qquad \text{(I)}$$

where, ΔD_{1000} = ring deflection at 1000°F (or T of interest)

D_{ring} = diameter of the ring alone at 1000°F (or T of interest)

$D_{comp.}$ = measured value of the ring-sample composite diameter at 1000°F (or T of interest).

The diameter of the ring alone at 1000°F was taken to be —

$$D_{ring} = D_o \, (1 + \alpha_r \Delta T) \qquad \text{(II)}$$

where, D_o = ring diameter at room temperature

α_r = ring average thermal expansion coefficient over T range of interest

ΔT = temperature deviation from room T.

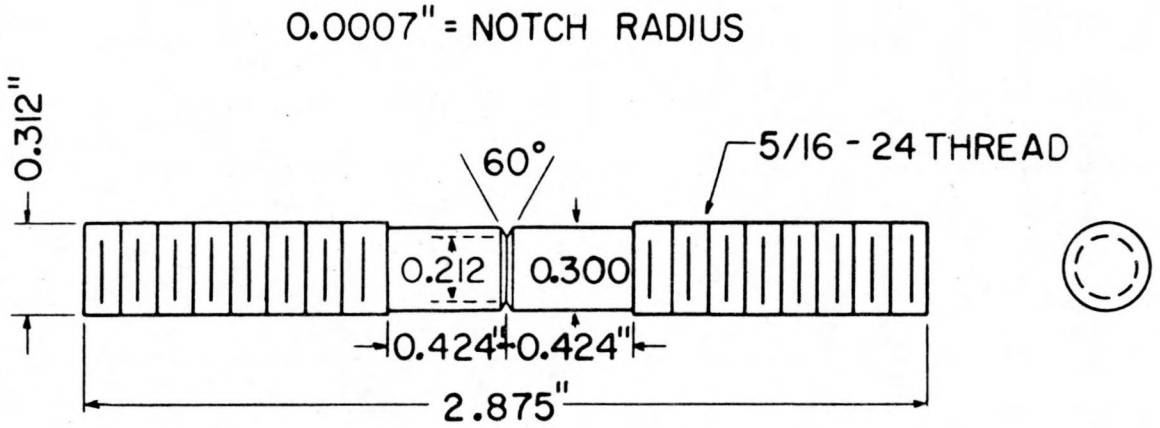

SCALE: 2" = 1"

Fig. 10: A387 Notched-Bar Tensile Specimen.

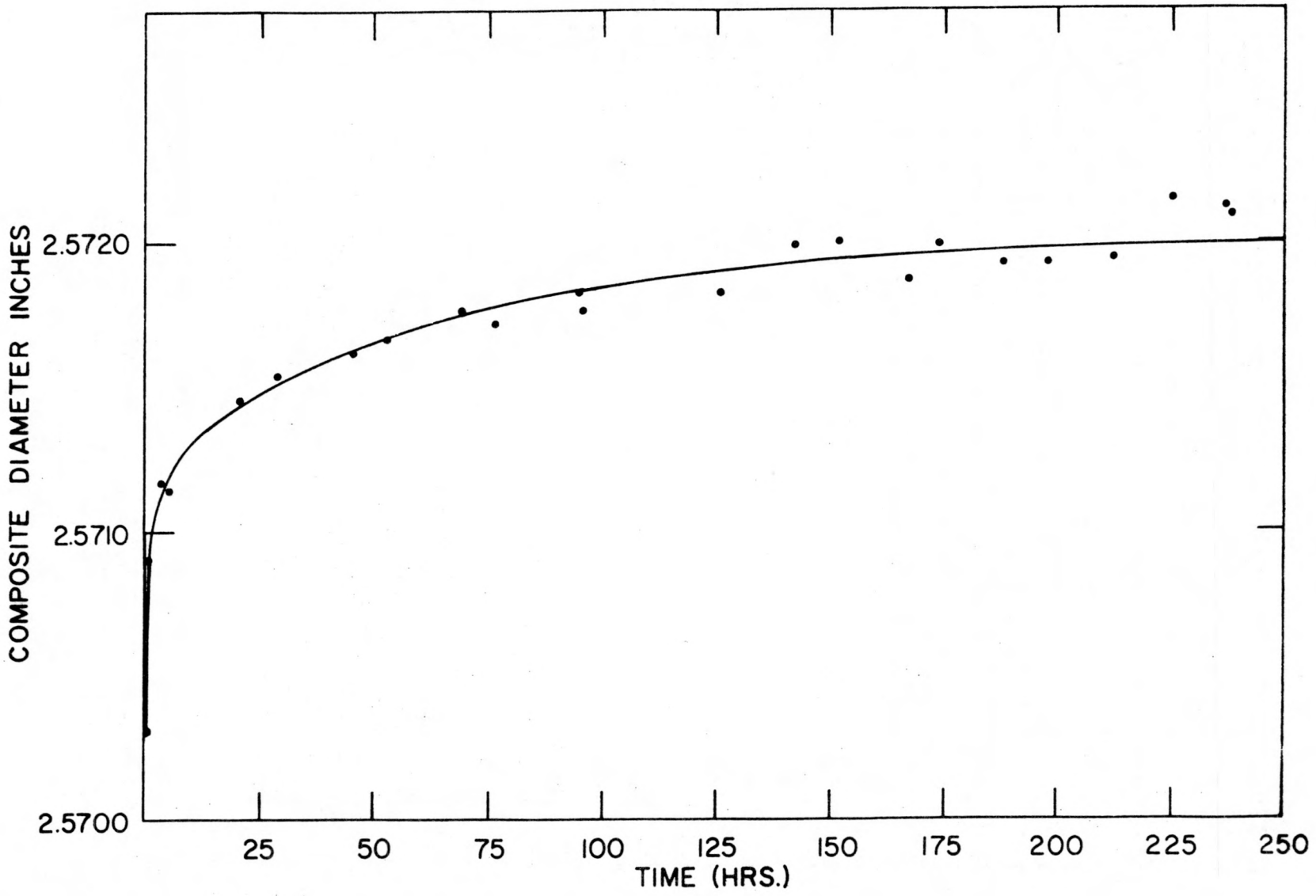

Fig. 11: Ring-Sample Composite relaxation vs. time at 1000°F in argon for an A387 notched-bar specimen initially loaded to 26.4 ksi.

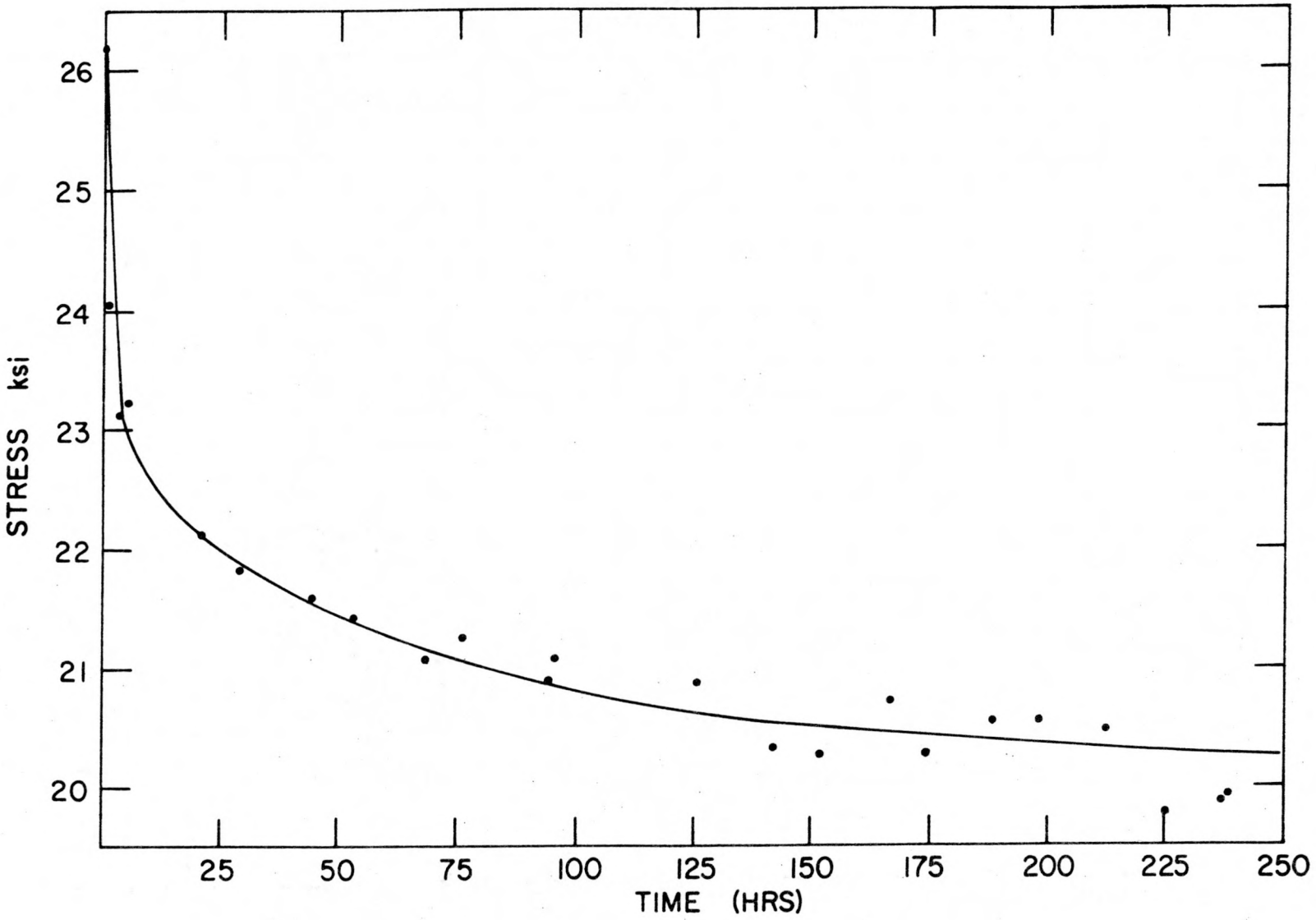

Fig. 12: Sample stress vs. time for an A387 notched-bar tensile specimen, ring loaded at 1000°F in argon.

Substituting Equation II into Equation I gives —

$$\Delta D_{1000} = D_o (1 + \alpha_r \Delta T) - D_{comp.} \qquad \text{(III)}$$

The load exerted by the ring on the specimen was —

$$P = K_r \Delta D_{1000} \qquad \text{(IV)}$$

where, P = Load

K_r = ring compliance coefficient at 1000°F (or T of interest).

The stress was then calculated by dividing the load by the thermally corrected cross-sectional area of the specimen, or —

$$\sigma = P/A \qquad \text{(V)}$$

where, σ = stress in the specimen

and,

$$A = A_o (1 + \alpha_s \Delta T)^2 \qquad \text{(VI)}$$

where, A = thermally corrected area of specimen

A_o = area at room temperature of specimen

α_s = specimen average thermal expansion coefficient over T range of interest.

Substituting Equations III, IV and VI into V resulted in the equation for the stress in the sample for any measured value of the ring-sample composite diameter —

$$\sigma = \frac{K_r(D_o(1 + \alpha_r \Delta T) - D_{comp.})}{A_o(1 + \alpha_s \Delta T)^2} \qquad \text{(VII)}$$

If the problem is treated as one of elastic equilibrium between two bodies (i.e. the sample and the ring) undergoing a thermal deviation from room temperature, the following equation of equilibrium is obtained —

$$\Delta D_T = \frac{\frac{A\,E}{\ell_\varepsilon}(D_o - \ell_s + \alpha_r D_o \Delta T - \alpha_s \ell_s \Delta T)}{K_r + \frac{A\,E}{\ell_\varepsilon}} \qquad \text{(VIII)}$$

where, ΔD_T = theoretical ring deflection at T of interest

E = Young's modulus of specimen at T of interest

ℓ_ε = straining gage length of specimen (effective gage length), thermally corrected

ℓ_s = length of specimen loaded in ring, this is a function of the initial room temperature ring deflection.

The derivation of Equation VIII is too lengthy to be presented here. However, the theoretically calculated value of deflection for a ring-sample composite having an initial room temperature deflection of 1.7×10^{-3} inches and heated to 1000°F is 7.63×10^{-3} inches. The experimentally determined value of ring deflection for the same conditions was 7.56×10^{-3} inches. Since the standard error is found to be $\pm 0.1 \times 10^{-3}$ inches for both cases, the difference is meaningless. The agreement between theory and experiment is very good.

The same relaxation test as outlined above was done at 950°F in argon for 350 hours. The relaxation and stress curves are presented in Figures

13 and 14 respectively.

Calibration curves of compression load versus deflection were determined for diametrically loaded rings of 316 stainless steel (Fig. 15). Tests were carried out in argon at 76, 200, 400, 600, 820 and 1000°F. Results are shown in Fig. 16. Ring compliance coefficients were determined from the slopes of the load-deflection curves. The results are plotted versus temperature in Fig. 17. The compliance coefficients showed linear behavior with temperature.

Bolt-loaded compact tension specimens (Fig. 6) were prepared from a 0.75 inch thick hot rolled plate of A387-74A-Gr.22-Cl.2 steel as described in Section I of this report. Three specimens were precracked (using the method outlined in Section I) to a total crack length, 'a' (as measured from the load line to the tip of the precrack), of 1.1843, 1.1950 and 1.2412 inches respectively.

Compliance curves were determined at room temperature for all three BLCTS and at 800°F for the two specimens with the longest total crack length. The compliance was measured at the notch front face (A, Fig. 6). Results are presented in Fig. 18. The ratio of the slopes of the compliance curves at 800°F to those at room temperature for each respective crack length equals (within experimental error) the ratio of Young's modulus of the material for the two temperatures.

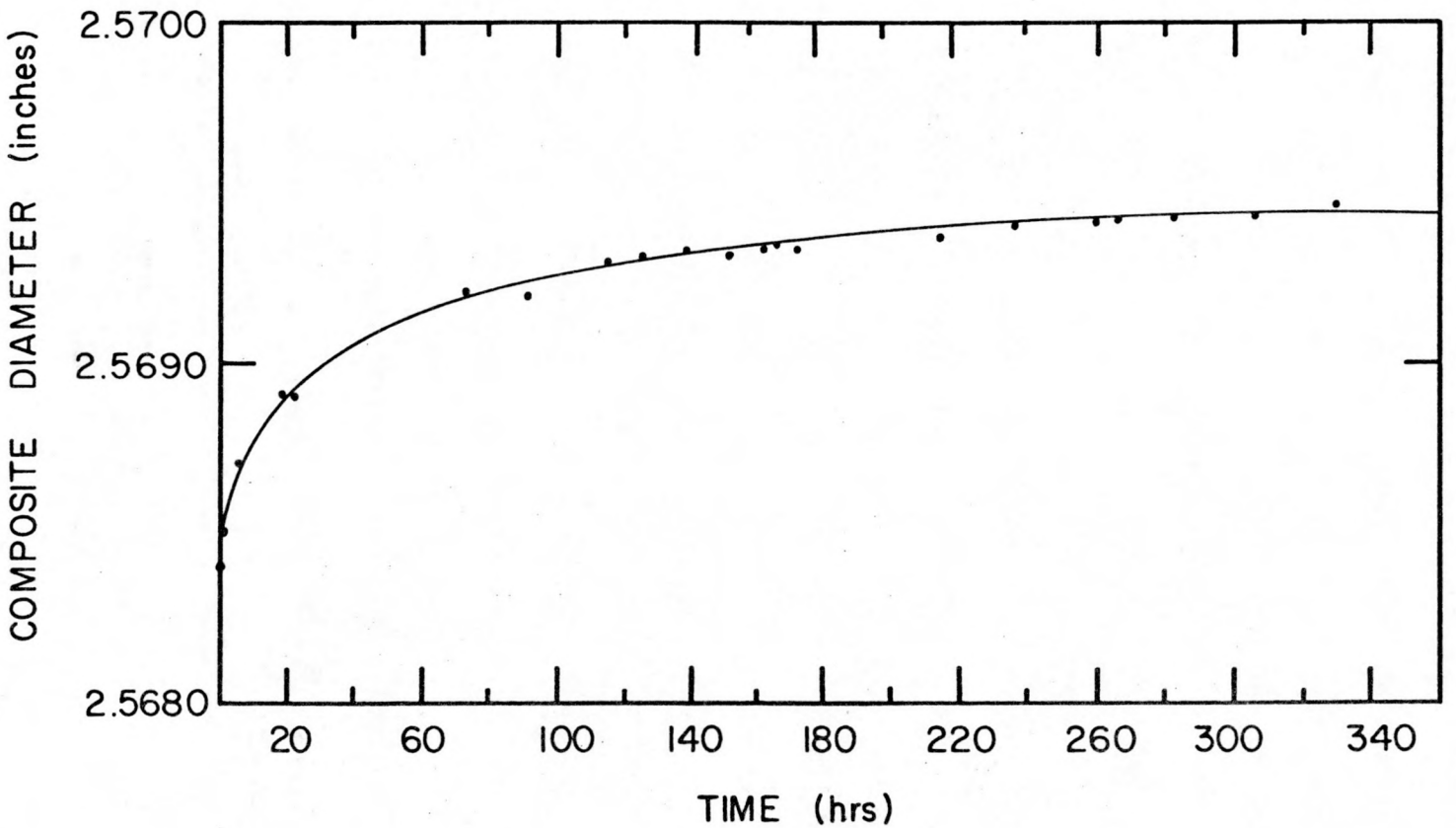

Fig. 13: Ring-sample composite relaxation vs. time at 950°F in argon for an A387 notched-bar specimen initially loaded to 24.0 ksi.

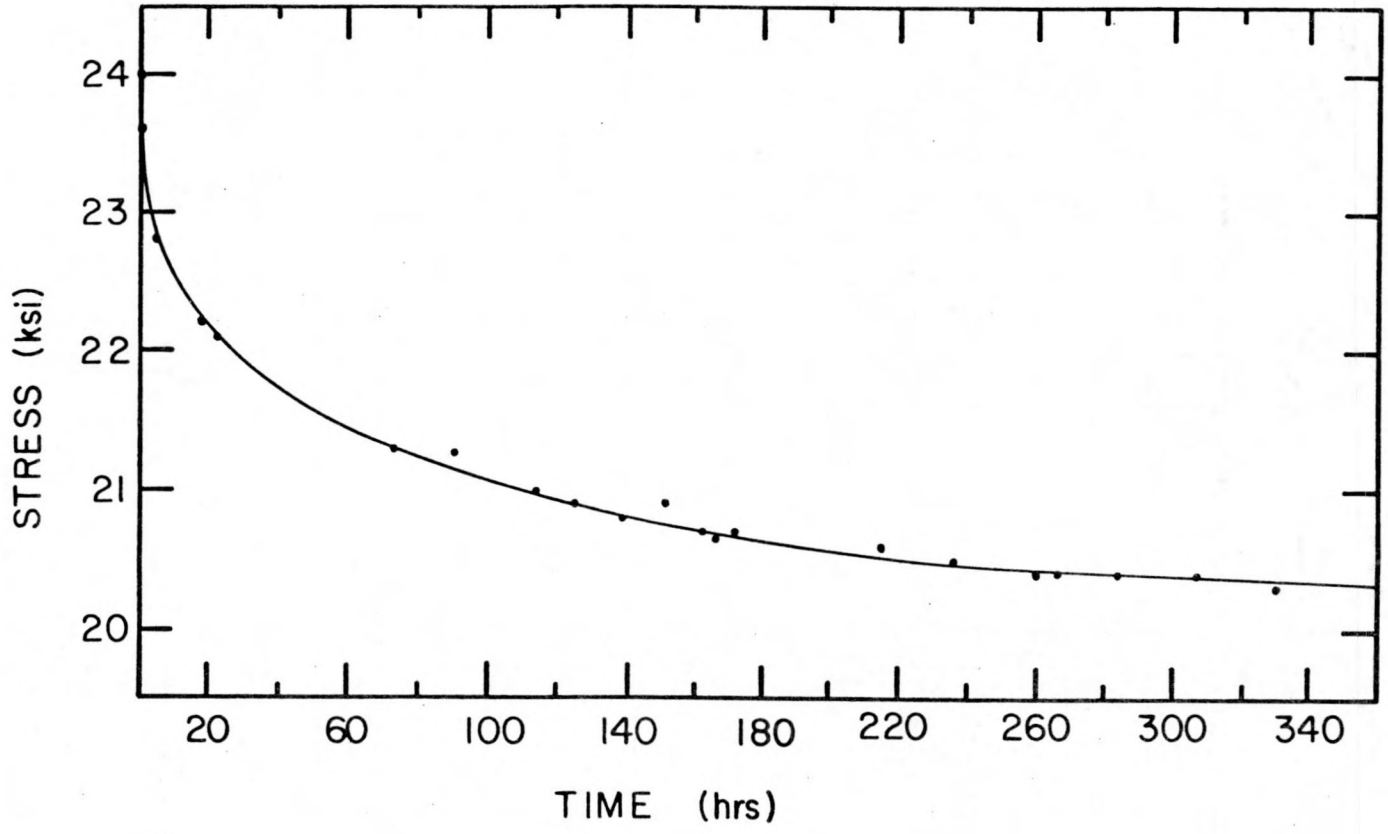

Fig. 14: Sample stress vs. time for an A387 notched-bar tensile specimen, ring loaded at 950°F in argon.

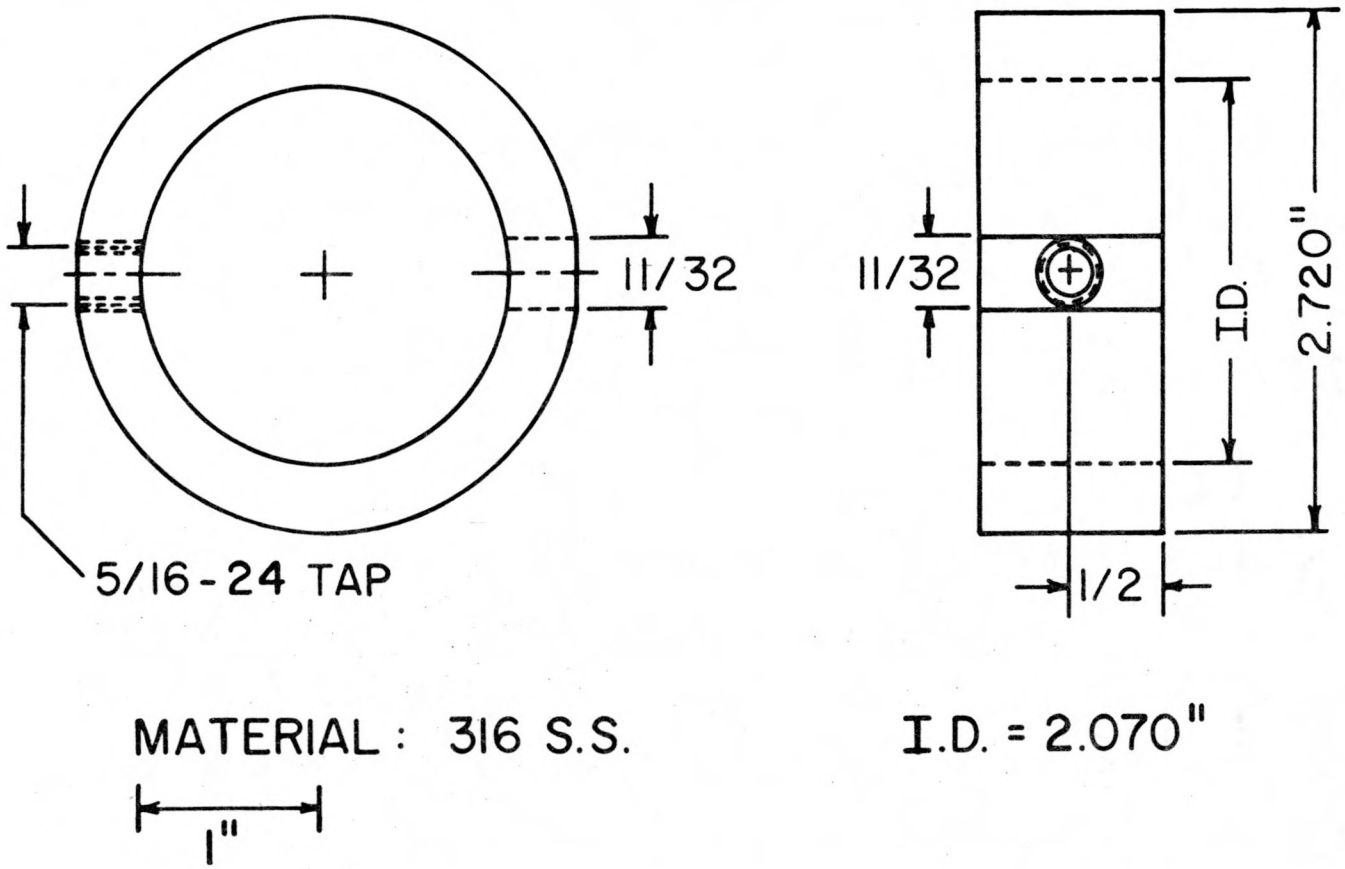

Fig. 15: 316 SS Loading Ring. Rings used in this study have O.D. = 2.554 inches.

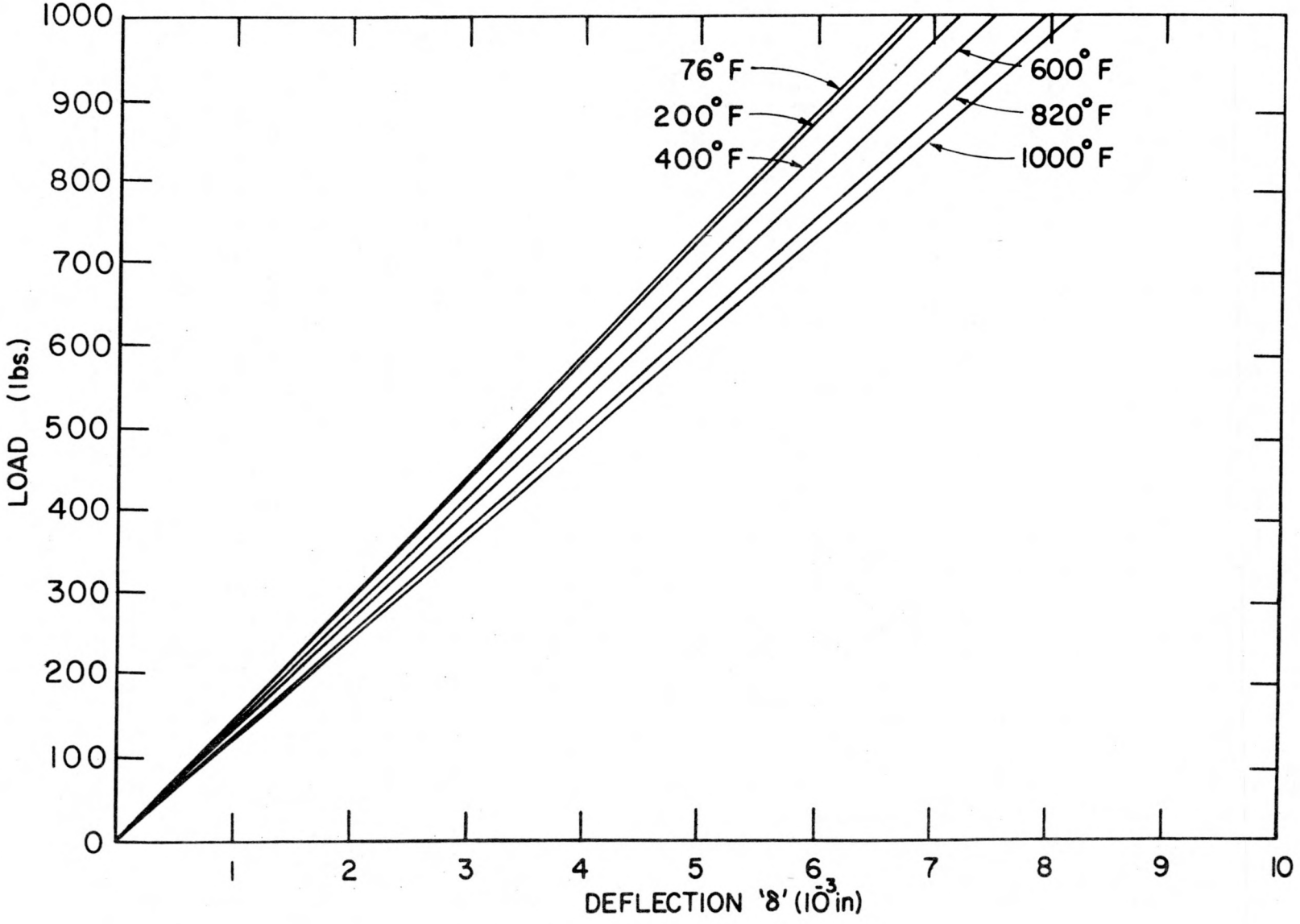

Fig. 16: 316 SS ring deflection vs. compression load calibration curves.

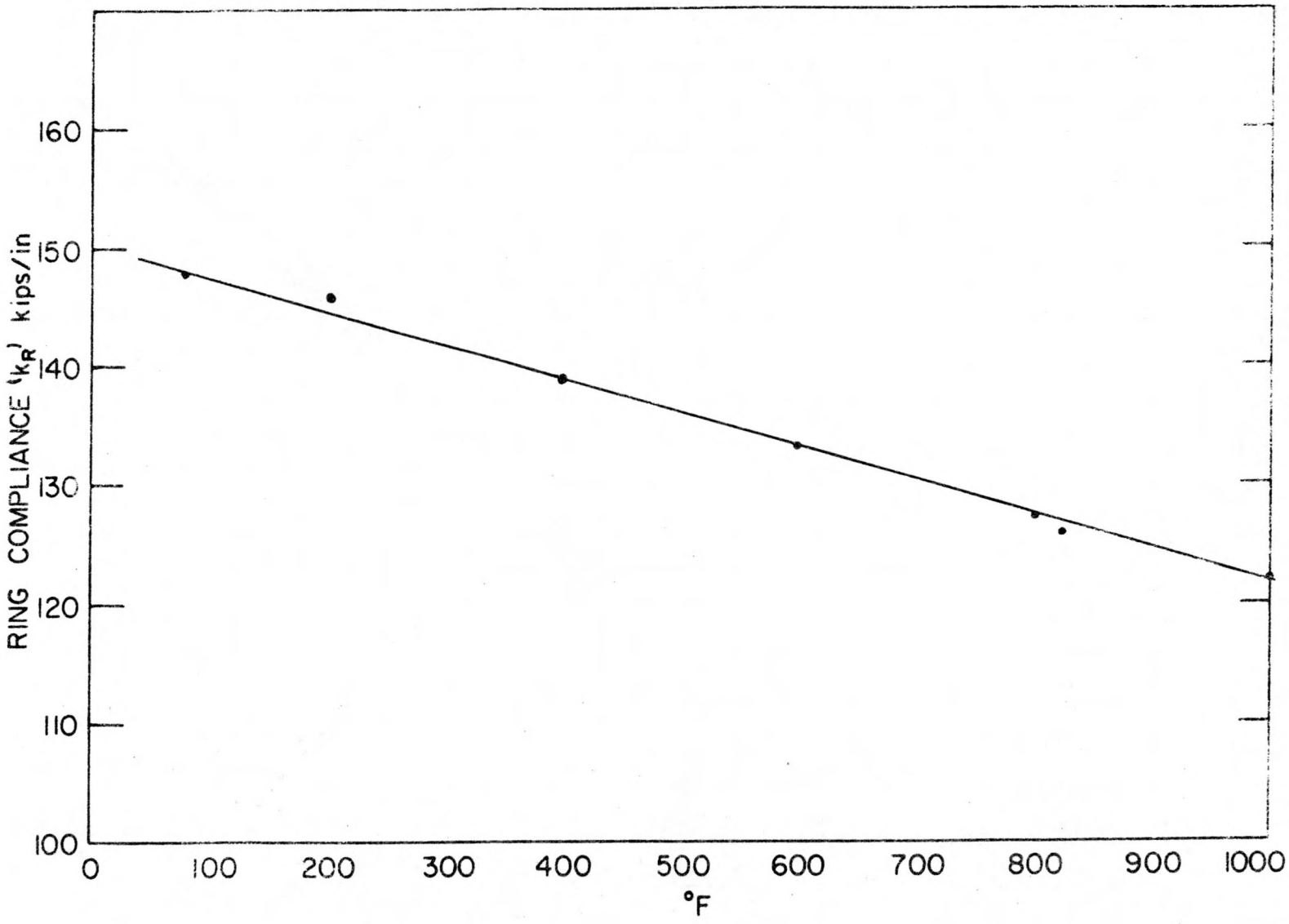

Fig. 17: 316 SS ring compliance coefficients vs. temperature.

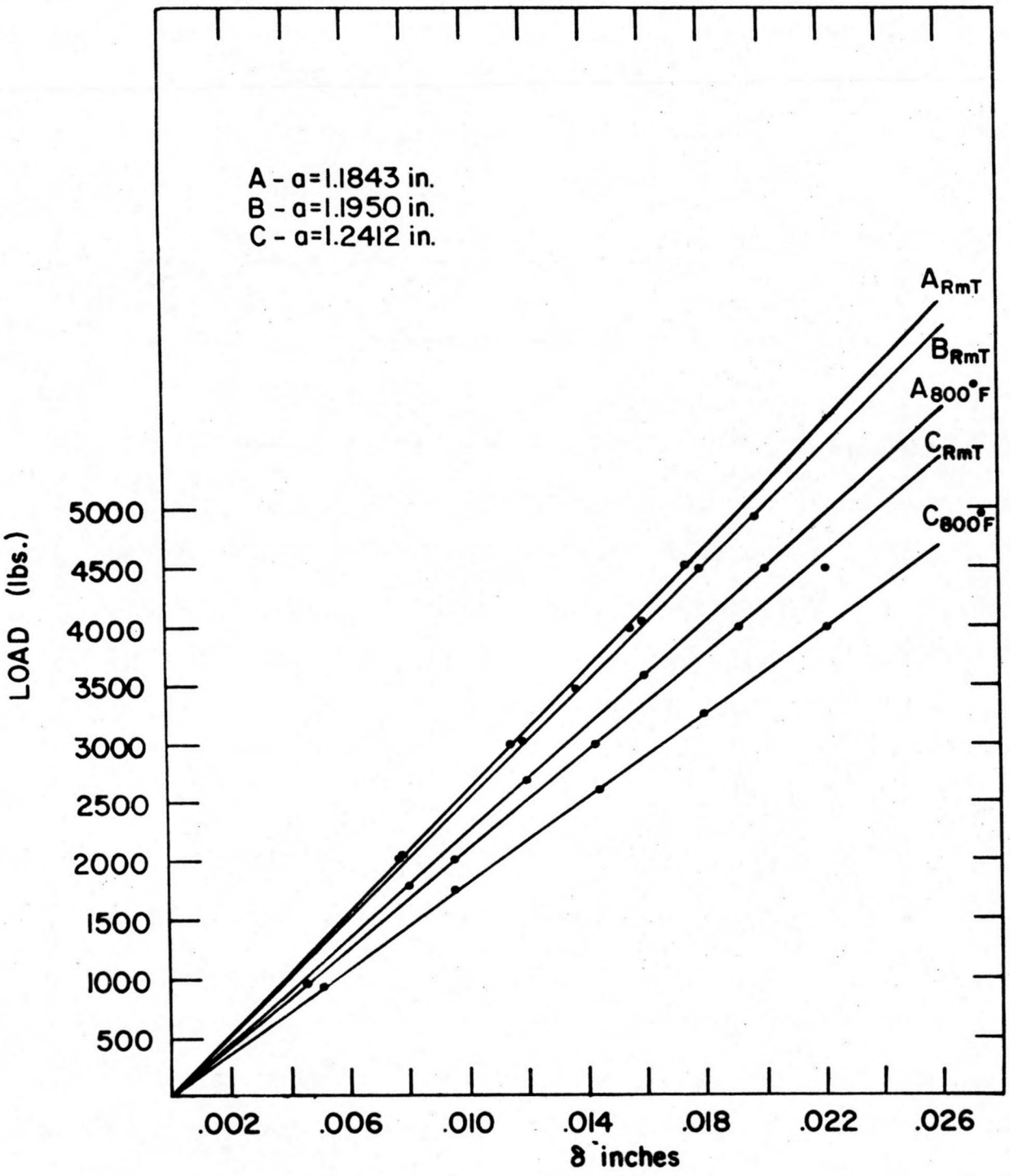

Fig. 18: Load vs. compliance (measured at the notch front face) for bolt-loaded compact tension specimens of different crack lengths (a).

III. Hydrogen Attack Tests

A. Procedure:

Smooth-bar (Fig. 19) and notched-bar (Fig. 10) tensile specimens of A387-74A-Gr.22-Cl.2 steel were prepared from longitudinal (parallel to the rolling direction) sections of the plate. Six smooth-bar and six notched-bar specimens were exposed to 4000 psig hydrogen gas at 1000°F for 500 hours. Three of each type of specimen were loaded under stress via precompressed stainless steel loading rings. Nine notched-bar specimens were exposed to 4000 psig hydrogen gas at 1000°F for 250 hours. Three specimens were stressed and six were unstressed during exposure. Three of the six unstressed samples had been prestrained (ε_p = 0.92%) in air at room temperature prior to the exposure. Three smooth-bar specimens were exposed unstressed to 4000 psig hydrogen gas at 1000°F for 168 hours. Seven notched-bar specimens were exposed to 4000 psig hydrogen gas at 950°F for 350 hours. Three specimens were stressed and four were unstressed during exposure. Two of the four unstressed samples had been prestrained (ε_p = 0.92%) in air at room temperature prior to the exposure.

Each type of exposure at 1000°F was done in three specimen lots. After the exposure the specimens were removed from the pressure vessel for analysis. One specimen of each lot was mounted in copper conducting bakelite and polished to Linde B (0.05 μ particle size) for micrographic analyses. The other two specimens of the lot were tensile tested at room temperature in air on a TT-C Instron tensile test machine. The unstressed samples of the 950°F test were tensile tested first and then mounted in copper conducting bakelite.

Sample lengths, diameters and ring-sample diameters were measured

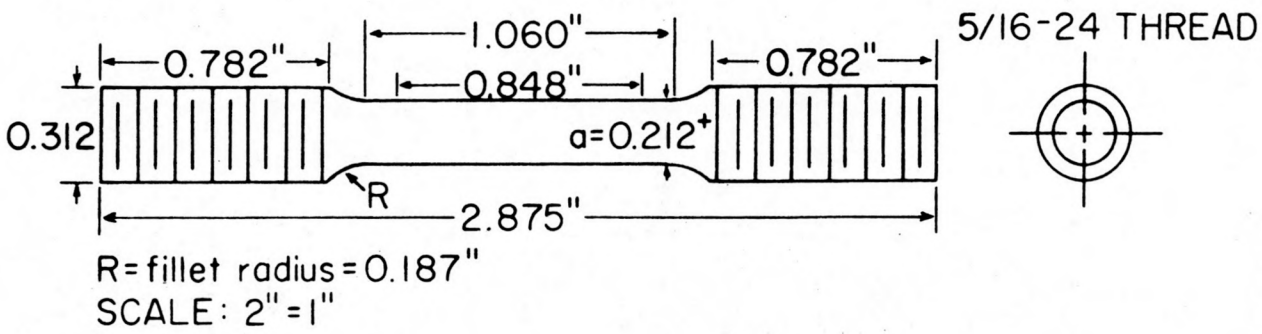

Fig. 19: A387 Smooth-Bar Tensile Specimen.

before and after the exposure. The stress in the stressed samples was calculated by —

$$\sigma = \frac{K_r \, \Delta D_T}{A} \qquad \text{(see Section II)} ,$$

ΔD_T was determined from measurements of ring deflection at the start and end of each exposure and by use of Equation VIII.

Metallographic analyses were performed both optically and with a scanning electron microscope (SEM). Surfaces were examined as polished and after etching for ∿10 seconds with a 2% Nital solution (2% HNO_3 in methanol).

B. Results:

Results of the mechanical properties tests on A387-74A-Gr.22-Cl.2 steel smooth-bar tensile samples pre-exposed to 4000 psig hydrogen gas at 1000°F are presented in Table 3. None of the room temperature mechanical properties were affected even after 500 hours of exposure.

Results of the mechanical properties tests on notched-bar samples of the same steel exposed to the same conditions of temperature and H_2 pressure as given above are presented in Table 4. No significant loss of notch tensile strength was observed except for the 500 hour stressed exposures. Considerable differences were noted in reduction of area (R.A.) for specimens exposed under conditions of stress and pre-strain. The 250 hour exposures showed no difference between R.A.'s for unstressed specimens exposed to argon or hydrogen. The stressed specimens exhibited ∿20% less R.A. for specimens exposed to hydrogen than those exposed to argon. The pre-strained samples showed ∿25% less R.A. for samples exposed to hydrogen than those exposed to argon. The 500 hour exposures exhibited degradation for

TABLE #3

MECHANICAL PROPERTIES TESTS

2 1/4 Cr-1 Mo steel smooth-bar tensile samples pre-exposed to 4000 psig H_2 at 1000°F

Test conditions: T=72°F P=1 atm air $\dot{\varepsilon}$=0.05 min^{-1}

Type of Exposure	Exposure Time (Hrs.)	Stress* (ksi)	ΔL/Lo** (%)	ΔD/Do*** (%)	0.2%Y.S. (ksi)	U.T.S. (ksi)	T.E. (%)	R.A. (%)
None (as-received)	---	----	----	--	78.7	95.6	24.7	75.5
Unstressed	168	----	0	0	79.5	96.0	23.2	74.2
Unstressed	500	----	0	0	78.5	95.0	23.0	75.4
Stressed	500	30.2 to 17.8	0.35	∿0	76.5	93.0	23.7	74.2

* Applied by pre-compressed loading rings. Values are for start of run and end of run.

** Change in sample length during exposure divided by sample gage length (1").

*** Change in sample gage diameter during exposure divided by original gage diameter.

TABLE #4

MECHANICAL PROPERTIES TESTS

2 1/4 Cr-1 Mo steel notched-bar tensile samples pre-exposed to 4000 psig H_2 at 1000°F

Test conditions: T=72°F P=1 atm air $\dot{\varepsilon}$=0.05 min^{-1}

Type of Exposure	Gas	Exposure Time (Hrs.)	Stress* (ksi)	L/Lo** (%)	D/Do*** (%)	N.T.S. (ksi)	R.A. (%)
None (as-received)	-----	---	----	----	----	148.2	25.0
Unstressed	H_2	250	----	0	+0.14	148.6	25.3
Stressed	H_2	250	26.4 to 19.4	+0.07	+0.05	147.3	20.4
Prestrained (0.92%)	H_2	250	----	0	+0.05	145.4	17.7
Unstressed	H_2	500	----	0	----	148.0	21.0
Stressed	H_2	500	31.2 to 19.7	+0.12	----	128.0	11.0
Unstressed	Argon	250	----	0	0	148.2	26.1
Stressed	Argon	250	26.4 to 20.1	+0.06	0	149.4	25.3
Prestrained (0.92%)	Argon	14	----	0	0	149.8	23.7

* Applied by pre-compressed loading rings. Values are for start of run and end of run.

** Change in sample length during exposure divided by total sample length (∿2.86").

*** Change in sample notch-diameter during exposure divided by original notch-diameter.

both the unstressed and stressed samples. There was no loss of strength for the unstressed samples. The stressed samples showed ∿13.5% less notch tensile strength than the as-received material. The reduction in area of the unstressed samples decreased by ∿16%, while the stressed samples showed ∿56% less reduction in area.

Results of the mechanical properties tests on samples exposed to 4000 psig H_2 gas at 950°F are presented in Table 5. The room temperature mechanical properties were not affected by the exposure with the exception of the prestrained samples reduction in area. It was decreased by ∿20% over the base property value.

Metallographic analyses of all the 250 hour and 500 hour exposures to hydrogen, at 1000°F, revealed the formation of small methane bubbles in or near grain boundaries and second phase precipitates. The highest concentration of bubbles was observed in the vicinity of the notch of stressed samples where the triaxiality of stress was greatest. Figures 20, 21 and 22 illustrate the above very well.

Metallographic analyses of all the 350 hour exposures to hydrogen at 950°F revealed only scarce bubble formation. It was only observed in the region of the notch of stressed samples and near second phase particles of stressed and prestrained samples. No bubble formation was found in unstressed samples.

In summary, smooth-bar tensile specimens showed no significant changes in any of the room temperature mechanical properties even though methane bubbles were detected in or around grain boundaries and second phase particles. Notched-bar specimens, however, showed marked changes in many of the room temperature mechanical properties. Methane bubbles formed more readily

TABLE #5

MECHANICAL PROPERTIES TESTS

2 1/4 Cr-1 Mo steel notched-bar tensile samples pre-exposed to 4000 psig H_2 at 950°F

Test conditions: T=72°F P=1 atm air $\dot{\varepsilon}=0.05\ min^{-1}$

Type of Exposure	Gas	Exposure Time (Hrs.)	Stress* (ksi)	ΔL/Lo** (%)	ΔD/Do*** (%)	N.T.S. (ksi)	R.A. (%)
Unstressed	H_2	350	----	0	0	150.2	22.6
Stressed	H_2	350	24.3 to 18.1	0.04	0	149.7	23.0
Prestrained	H_2	350	----	0	0	149.6	20.5
Stressed	Argon	350	24.0 to 20.1	0.03	0	149.7	24.2

* Applied by pre-compressed loading rings. Values are for start of run and end of run.

** Change in sample length during exposure divided by total sample length (≈2.86").

*** Change in sample notch-diameter during exposure divided by original notch-diameter.

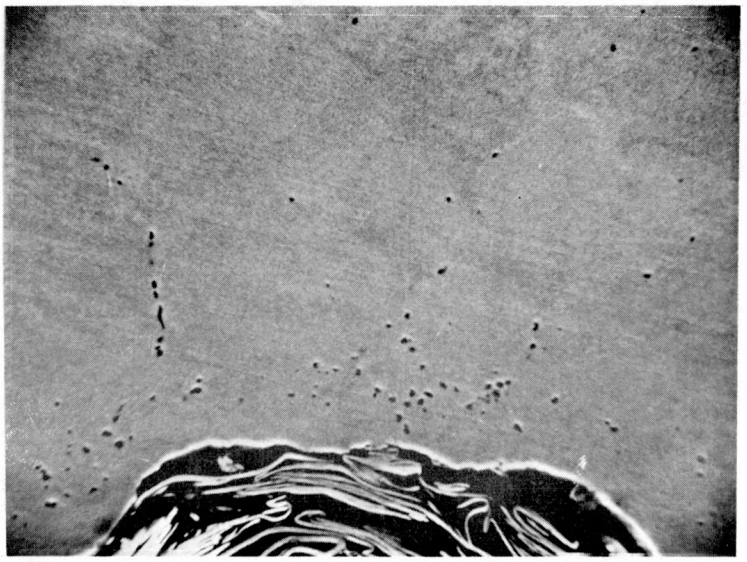

Fig. 20: Scanning electron micrograph showing high density of bubbles in region of notch for A387 notched-bar tensile specimen exposed with stress for 500 hours to 4000 psig H_2 gas at 1000°F. (1260X)

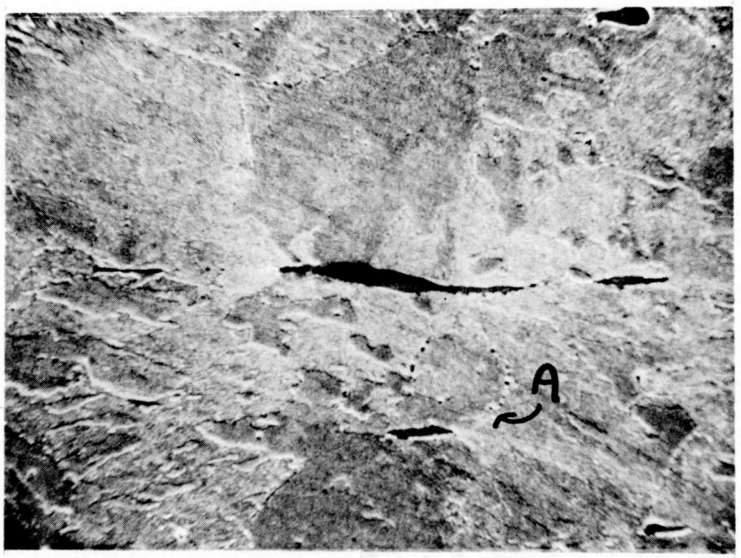

Fig. 21: Scanning electron micrograph of bulk region away from notch for specimen of Fig. 20. Surface was etched with 2% Nital (∿10 sec.). Bubbles are visible in grain boundaries and near the manganese sulfide precipitates. (1000X)

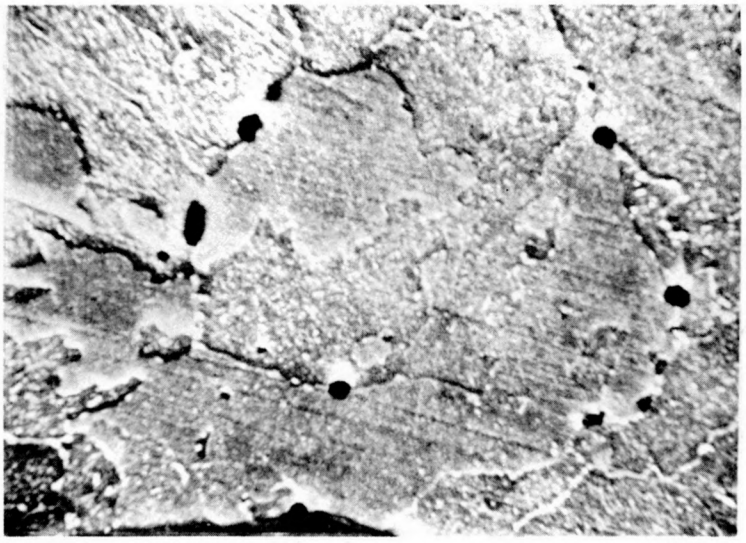

Fig. 22: Scanning electron micrograph of region A in Fig. 21 at higher magnification (5000X). Shows bubbles in grain boundaries and on interface between manganese sulfide inclusion and bulk matrix (bottom center).

in regions of high stress triaxiality. The great loss of reduction in area for the prestrained samples indicates that it may be strain and not stress that causes the increased amount of hydrogen attack in the vicinity of the notch.

IV. Corrosion Tests

A. Procedure:

Cylindrical corrosion specimens (Fig. 23) were prepared from longitudinal (parallel to the rolling direction) sections of the plate. One group each of 4 specimens was placed in a pressure vessel and subjected to one of the following exposures: 24, 48, 72 or 240 hours in a coal slurry and hydrogen gas environment at 4000 psig pressure at 800°F. The coal slurry was the same as that described in Section I of this report.

Two samples of each group were immersed in the coal slurry, which was contained inside a 304 stainless steel can, and the remaining two samples were suspended in the gaseous phase above the slurry. The can was then placed inside one of the specially designed H_2 pressure vessels for subsequent pressure and temperature equilibration. The samples were exposed to conditions given above during which time the total pressure was controlled within ±100 psig of the required pressure. The temperature fluctuations were ±10°F.

At the end of each exposure the samples were removed from the pressure vessel, cleaned with acetone and mounted in conducting Bakelite. The samples were then ground and polished to Linde B (.05 micron particle size Al_2O_3). Care was taken to keep the sample surface parallel to the Bakelite base. The scale thickness was then microscopically measured. The

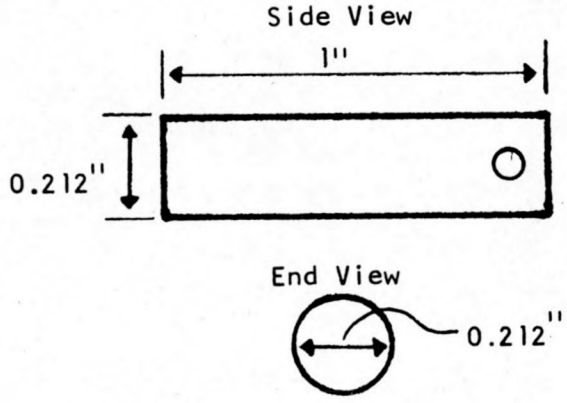

Fig. 23: 2 1/4 Cr-1 Mo Steel Corrosion Specimen.

measurements were done on the ends of the samples to assure measurement of a perpendicular cross section. Six measurements of each specimen were made at random and the values for each two like specimens (i.e. gas phase or slurry immersion exposures) were averaged. Micrographs were then made of each set of samples.

B. Results:

Results of the corrosion tests are given in Figures 24 through 30. A linear plot of scale thickness vs. exposure time (Fig. 24) shows what appears to be a parabolic growth rate curve. However, when the data are plotted as scale thickness vs. log time (Fig. 25) the result is a straight line. The scale thickness of a smooth-bar tensile specimen immersed in the slurry and exposed to the same exposure conditions for 856 hours falls on the log t vs. thickness line for the specimens that were suspended in the slurry gases. Also, the 240 hour slurry immersed samples show scale growth only slightly less than the 240 hour suspended samples whereas the 24, 48, and 72 hour tests show markedly slower scale formation rates in the slurry phase than in the slurry gas phase (Fig. 25).

It has been our experience that during the course of the first 168 hours of 800°F exposures to the coal slurry environment, the slurry undergoes marked changes as the heavy viscous portions of the slurry react with the hydrogen to form lighter fractions. These light fractions cause an increase in pressure above the upper pressure control point and get vented off via the pressure release system. After about 168 hours the system stabilizes and remains reasonably constant in pressure. What is then present is a mixture of slurry gases, H_2, some light liquids and coke.

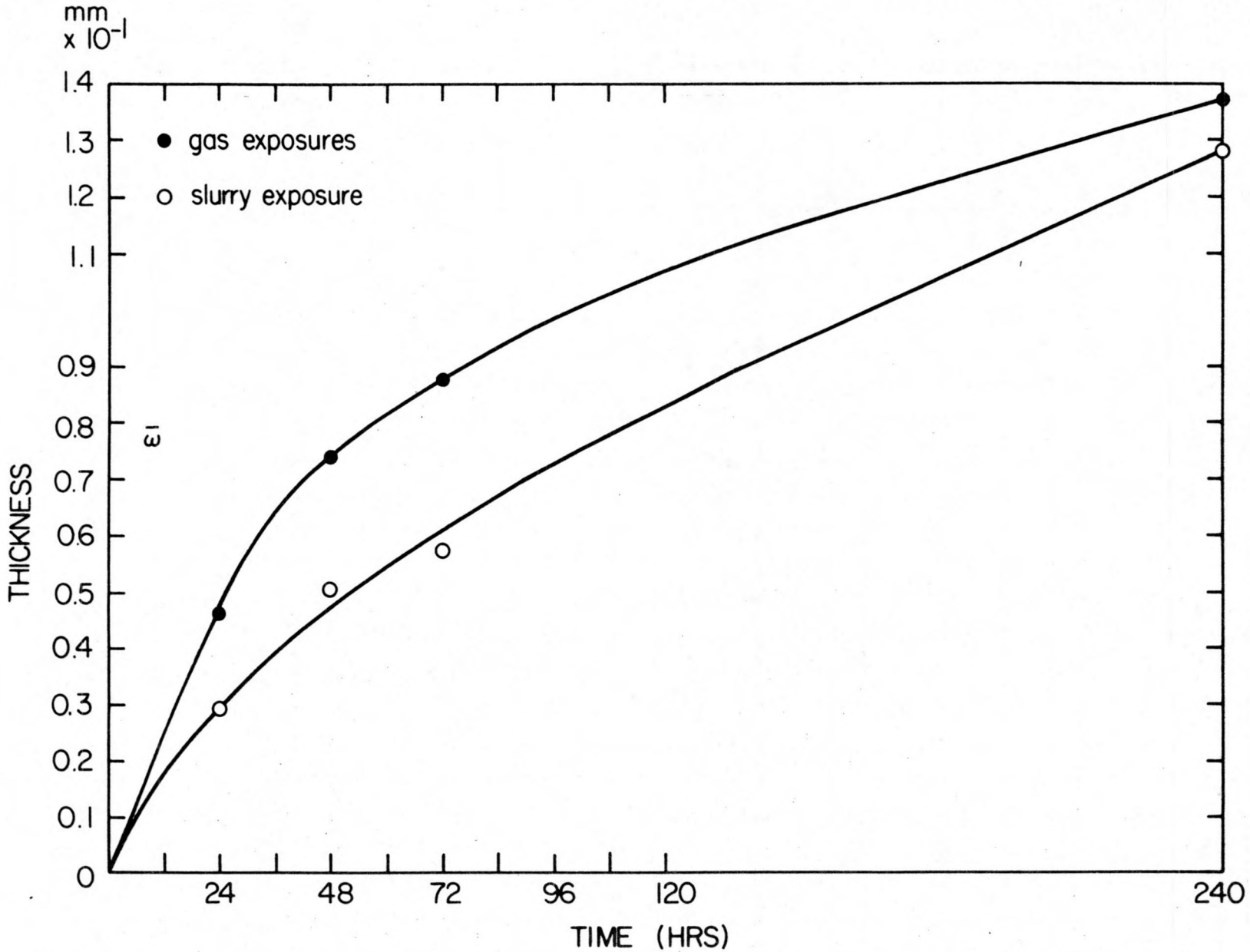

Fig. 24: Surface scale thickness vs. time plot for 2 1/4 Cr-1 Mo steel exposed to a coal slurry-H_2 environment at 800°F and 4000 psig total pressure.

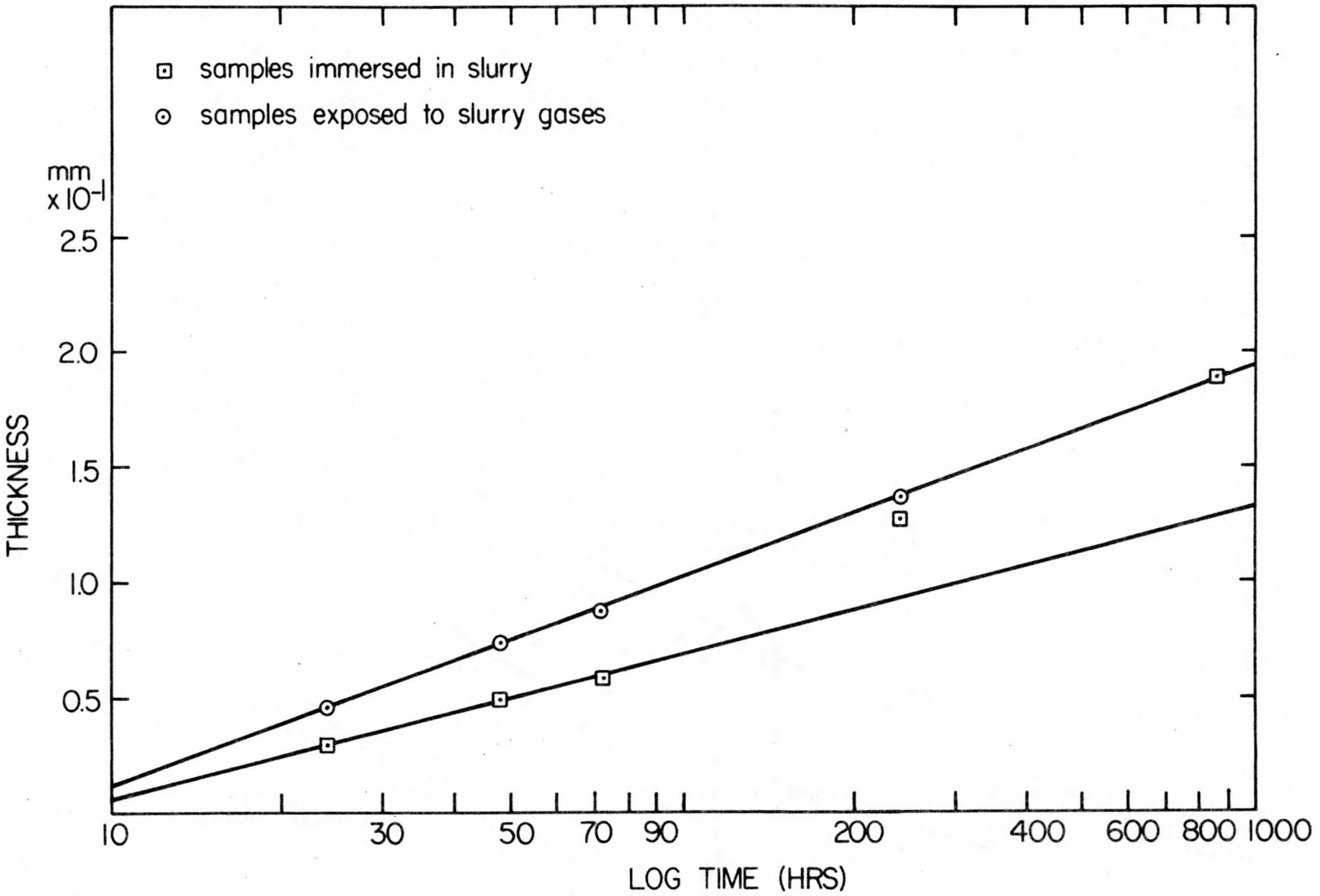

Fig. 25: Surface scale thickness vs. log time plot for 2 1/4 Cr-1 Mo steel exposed to a coal slurry-H_2 environment at 800°F and 4000 psig total pressure.

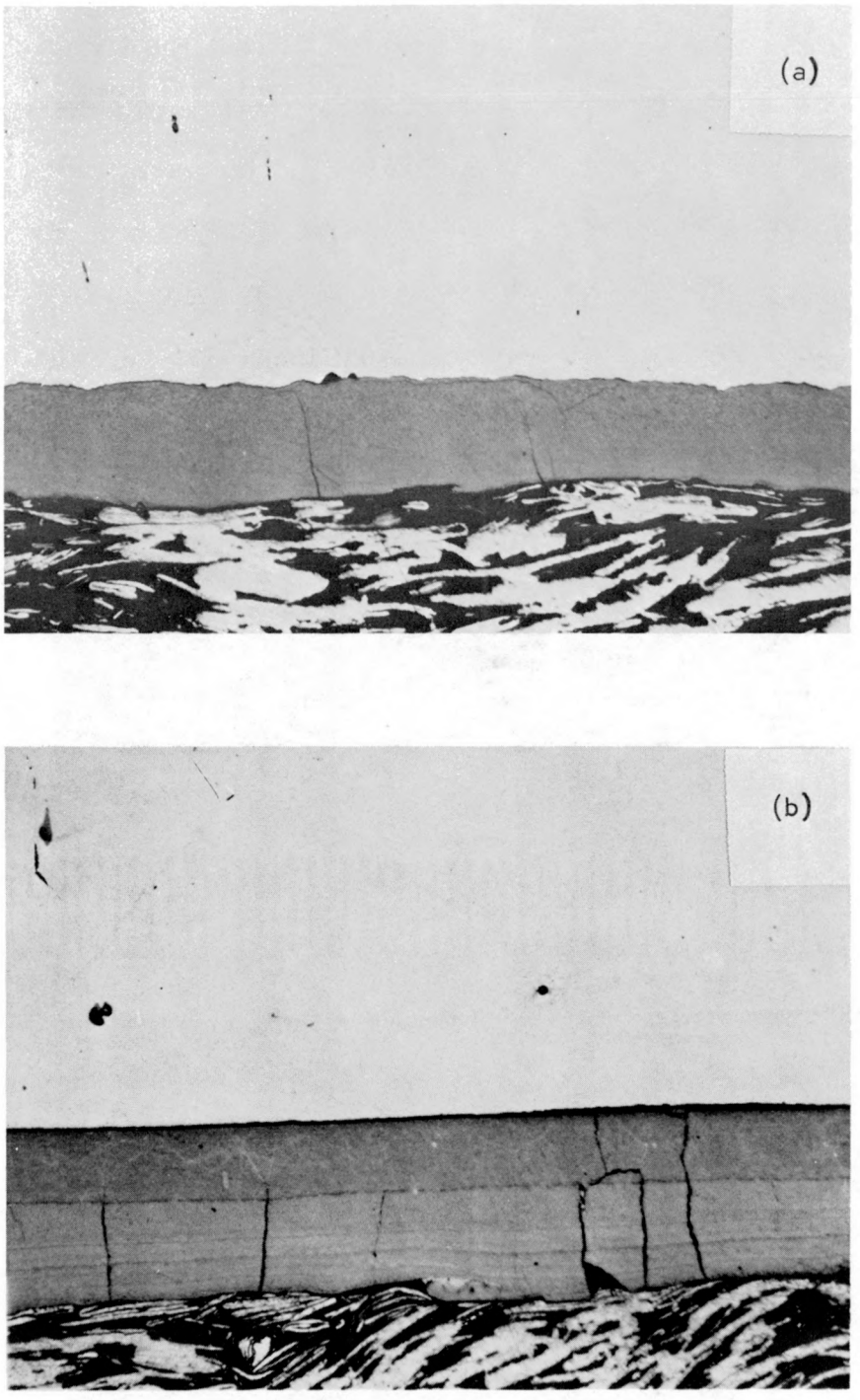

Fig. 26: Surface scale region of 2 1/4 Cr-1 Mo steel exposed to a coal slurry-H_2 environment at 800°F, 4000 psig pressure for 24 hours. a.) Immersed in slurry. b.) Suspended in gas phase. (500X)

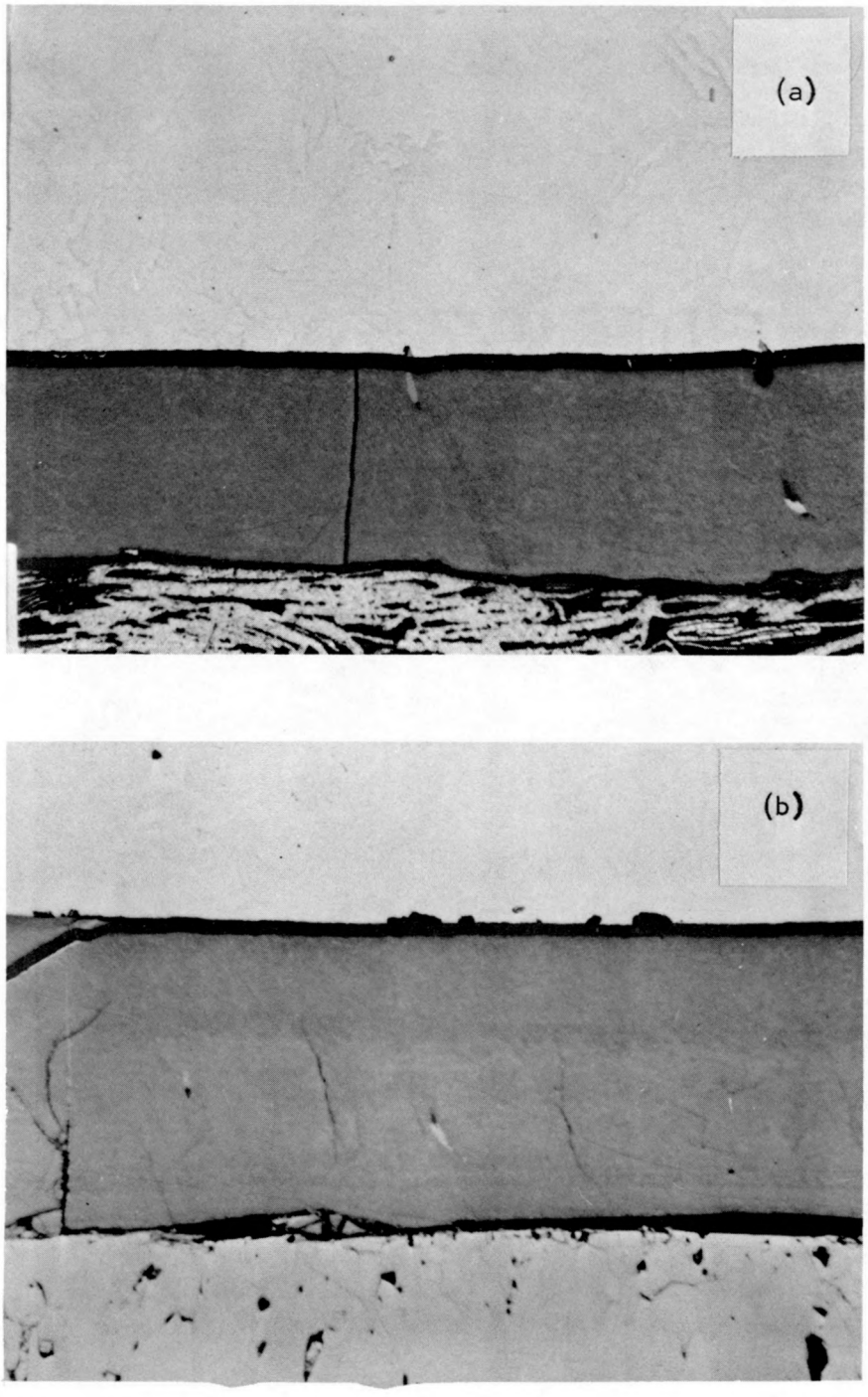

Fig. 27: Surface scale region of 2 1/4 Cr-1 Mo steel exposed to a coal slurry-H_2 environment at 800°F, 4000 psig pressure for 48 hours. a.) Immersed in slurry. b.) Suspended in gas phase. (500X)

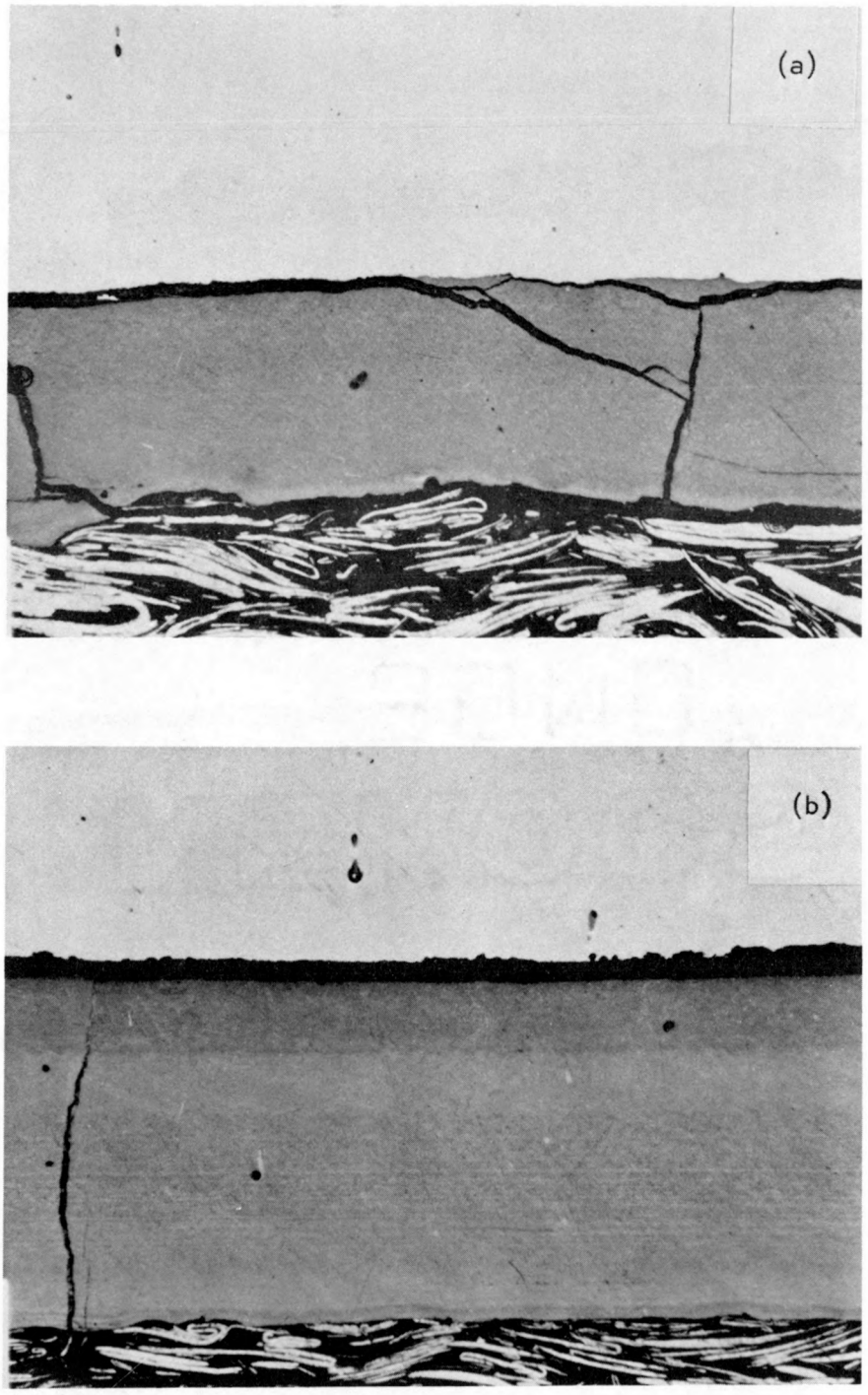

Fig. 28: Surface scale region of 2 1/4 Cr-1 Mo steel exposed to a coal slurry-H_2 environment at 800°F, 4000 psig pressure for 72 hours. a.) Immersed in slurry. b.) Suspended in gas phase. (500X)

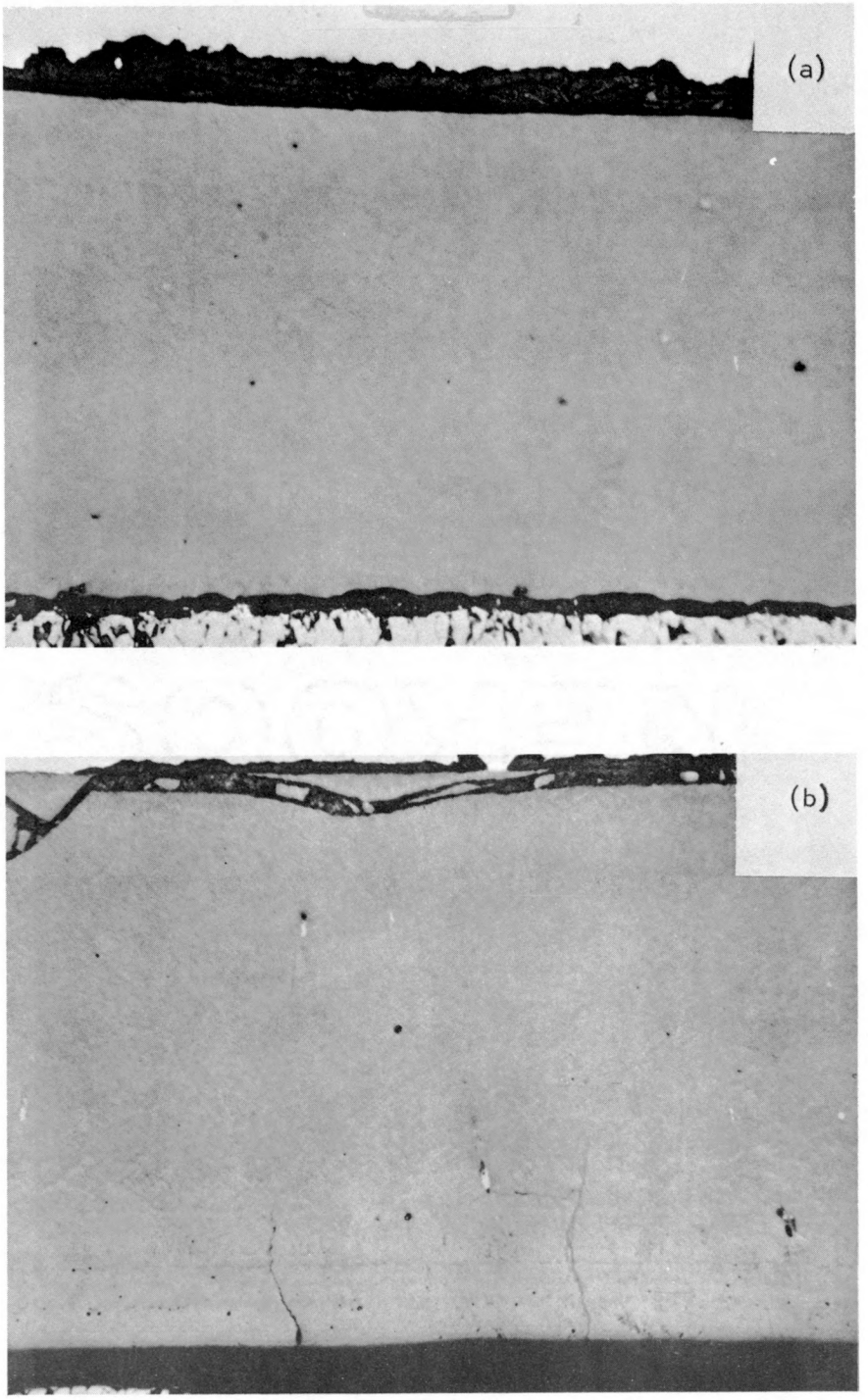

Fig. 29: Surface scale region of 2 1/4 Cr-1 Mo steel exposed to a coal slurry-H_2 environment at 800°F, 4000 psig pressure for 240 hours. a.) Immersed in slurry. b.) Suspended in gas phase. (500X)

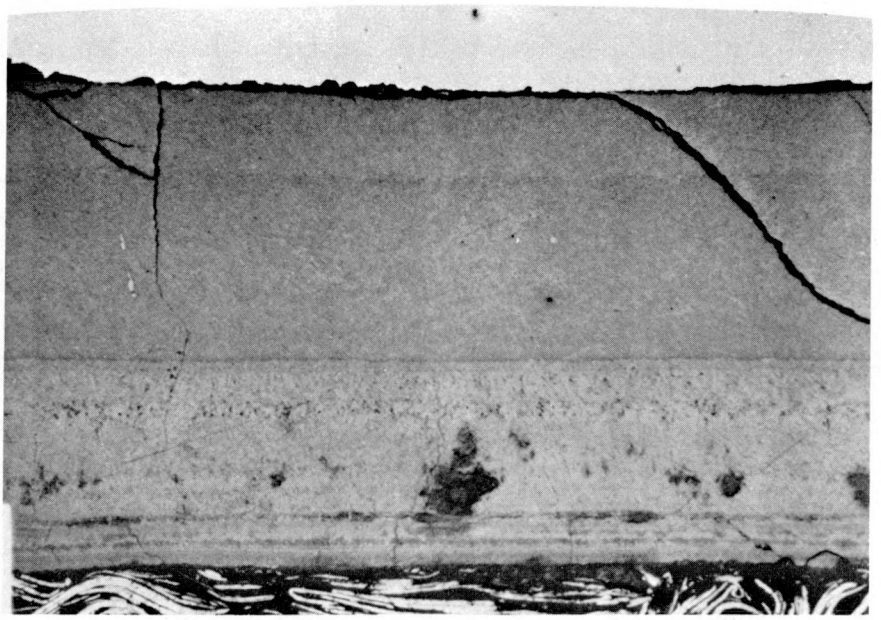

Fig. 30: Surface scale region of 2 1/4 Cr-1 Mo steel exposed to a coal slurry-H_2 environment at 800°F, 4000 psig pressure for 240 hours. The specimen was suspended in the slurry gas phase. Different regions of scale composition can be seen. (500X)

Therefore, for the short time exposures, the mobility of the corrosive species is probably hindered by the heavy viscous fractions of the slurry and results in slower scale formation rates. As the viscous fractions are converted to light fractions, the mobility of the corrosive species increases which results in an increase in the scale formation rate approaching that in the gaseous phase. The scale formation rate is seen to be a logarithmic function of the exposure time in both phases (Fig. 25).

Electron microprobe analyses have been completed on some of the scales of the sequence. The total sequence is not yet completed so it will not be discussed in this report.

V. Coal Analyses

Four specimens were selected from the 55 gallon drum of 100 mesh Kentucky bituminous and analyzed for total sulfur and chlorine content. Likewise, three samples were drawn off from the 55 gallon drum of coal oil and analyzed for total sulfur and chlorine content. The results are listed in Table 6.

VI. Phase Stability Diagrams

A. Procedure:

The stability of a phase that can exist in equilibrium with its surroundings can be calculated in the following manner making use of the Gibb's free energy function. For any reaction of the form:

$$\nu_{r1} R_1 + \nu_{r2} R_2 + \cdots \rightarrow \nu_{p1} P_1 + \nu_{p2} P_2 + \cdots$$

the change in free energy for the reaction can be expressed as:

TABLE #6

COAL ANALYSES

Sample #	Total Sulfur (wt %)	Total Chlorine (wt %)
CMWCS-01A	5.66	0.03
CMWCS-01B	5.69	0.02
CMWCS-02A	5.66	0.03
CMWCS-02B	5.58	0.04
CMWCS-03A	5.39	0.06
CMWCS-03B	5.40	0.06
CMWCS-04A	5.49	0.04
CMWCS-04B	5.40	0.04
AVERAGES	5.53	0.04

COAL OIL ANALYSES

CMWCO-01	0.64	0.07
CMWCO-02	0.64	0.04
CMWCO-03	0.64	0.03
AVERAGES	0.64	0.05

$$\Delta G_{RXN} = \Sigma\ \nu_{pi}\ G_{pi} - \Sigma\ \nu_{ri}\ G_{ri} \qquad (I)$$

where, ν_i = stoichiometric coefficients

G_i = molar free energy of species i.

If we then define a standard state temperature and pressure, Equation I can be rewritten as follows:

$$\Delta G_{RXN} = \Delta G^{o,T_B}_{RXN} + \sum^{i} \int_{T_B}^{T} (-S_{pi}\ dT) - \sum^{i} \int_{T_B}^{T} (-S_{ri}\ dT)$$

$$+ \sum^{i} \int_{P_B}^{P} V\ dP_{pi} - \sum^{i} \int_{P_B}^{P} V\ dP_{ri} + \Delta\bar{G}_m \qquad (II)$$

where, $\Delta G^{o,T_B}_{RXN}$ = free energy change for the reaction at some standard T_B and P_B

T_B, P_B = standard state T and P, T_B = 298°K, P_B = 1 atm

$\int_{T_B}^{T} (-SdT)$ = temperature correction term for deviations from standard state to T of interest

$\int_{P_B}^{P} V\ dP$ = pressure correction term for deviation from standard state to P of interest

$\Delta\bar{G}_m$ = free energy of mixing.

If we 1.) combine the temperature correction terms with $\Delta G^{o,T_B}_{RXN}$,

2.) use as the equation of state PV = n RT for gaseous elements,

and 3.) neglect the effects of compressibility terms for all condensed species,

Equation II becomes —

$$\Delta G_{RXN} = \Delta G^{o,T}_{RXN} + RT\ (\Sigma\ \nu_{pi}\ \ln\ P - \Sigma\ \nu_{ri}\ \ln P) + \Delta \bar{G}_m \qquad \text{(III)}$$

where, $\Delta G^{o,T}_{RXN}$ = free energy change for the reaction at temperature, T, and standard state pressure, P_B.

The second term in Equation III expresses the sum of the pressure correction terms for all gaseous species. The third term, $\Delta \bar{G}_m$, can be expressed in the following way:

$$\Delta \bar{G}_m = RT\ (\overset{i}{\Sigma}\ \nu_{pi}\ \ln\ a_{pi} - \overset{i}{\Sigma}\ \nu_{ri}\ \ln\ a_{ri}) \qquad \text{(IV)}$$

where a_i is the activity of component i.

The activity of any gaseous species in a mixture of gases can be written as the product of the mole fraction of that gas, N_i, times an activity coefficient, γ_i, which describes the behavior of the gas with concentration.

$$a_{i\ gas} = \gamma_i N_i \qquad \text{(V)}$$

The free energy of mixing for the gas can now be expressed as follows:

$$\bar{G}_{m_i} = \nu_i RT\ \ln\ \gamma_i N_i\ . \qquad \text{(VI)}$$

Combining Equation VI with the pressure correction term for the gas results in the following equality:

$$\nu_i\ RT\ \ln\ \gamma_i N_i + \nu_i\ RT\ \ln\ P = \nu_i\ RT\ \ln\ \gamma_i N_i\ P \qquad \text{(VII)}$$

where, $\gamma_i N_i\ P = P_i$ = partial pressure of gas i.

Substituting Equations IV and VII into Equation III yields —

$$\Delta G_{RXN} = \Delta G^{o,T}_{RXN} + RT \left(\Sigma \nu_{pi} \ln P_{pi} - \Sigma \nu_{ri} \ln P_{ri}\right)$$

$$+ RT \left(\Sigma \nu_{pi} \ln a_{pi} - \Sigma \nu_{ri} \ln a_{ri}\right) \qquad \text{(VIII)}$$

The second term in Equation VIII denotes the sum of the combined pressure correction and free energy of mixing terms for all gaseous species. The third term in Equation VIII denotes the sum of the free energy of mixing terms for all condensed species.

Applying Equation VIII to the reaction —

$$3Fe + 2O_2 \rightarrow Fe_3O_4 ,$$

gives —

$$\Delta G_{RXN} = \Delta G^{o,T}_{Fe_3O_4} - 2RT \ln P_{O_2} + RT \left(\ln a_{Fe_3O_4} - 3 \ln a_{Fe}\right) .$$

Combining terms —

$$\Delta G_{RXN} = \Delta G^{o,T}_{Fe_3O_4} + RT \ln \frac{a_{Fe_3O_4}}{(a_{Fe})^3 (P_{O_2})^2} \qquad \text{(IX)}$$

where, $\Delta G^{o,T}_{Fe_3O_4}$ = free energy of formation of Fe_3O_4 at temperature, T.

Assuming unit activity for Fe and Fe_3O_4, and assuming equilibrium conditions (i.e. $\Delta G_{RXN} = 0$) one obtains —

$$\Delta G^{o,T}_{Fe_3O_4} = -RT \ln \frac{1}{P_{O_2}^{\,2}}$$

or, $\Delta G^{o,T}_{Fe_3O_4} = 2RT \ln P_{O_2}$. (X)

Equation X allows the calculation of the partial pressure of O_2 above which Fe_3O_4 will form (i.e. $\Delta G_{RXN} < 0$).

Following with the outlined procedure it is possible to calculate the equilibrium thermodynamic phase stability boundaries between phases of interest at any temperature.

B. Results:

Phase stability diagrams have been constructed for Fe, Cr, Mo, and Mn in H_2S/H_2-O, H_2S/H_2-C, and C-O environments at 800°F (700°K). They are presented in Figures 31-40. It must be noted here that these diagrams in no way represent predictions of phases that will be present under the conditions of temperature and pressure stated therein. They merely illustrate the regions of thermodynamic stability of the various phases and act as an aid for interpreting data.

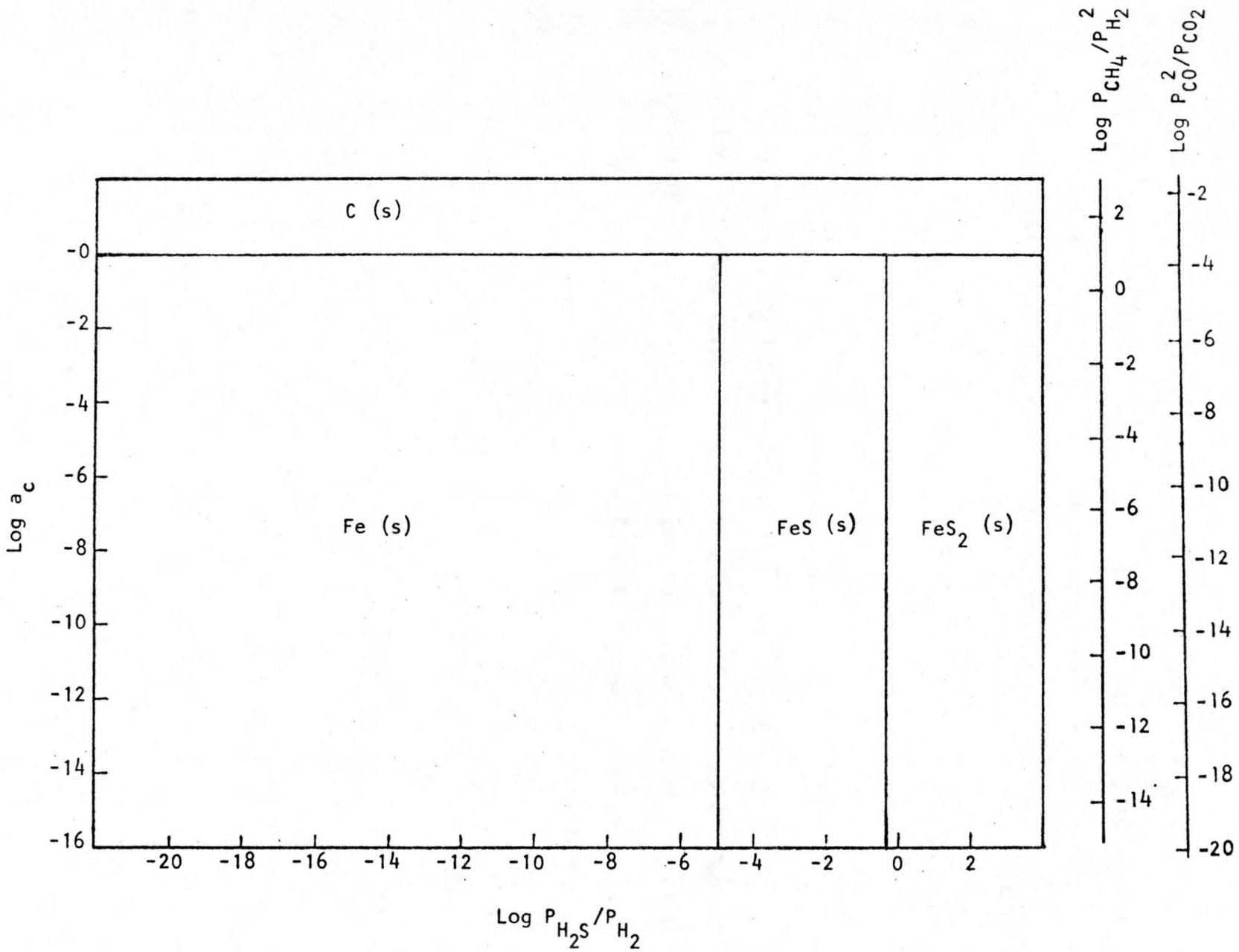

Fig. 31: Phase Stability Diagram: Fe-C-H_2S/H_2 at 800°F (700°K).

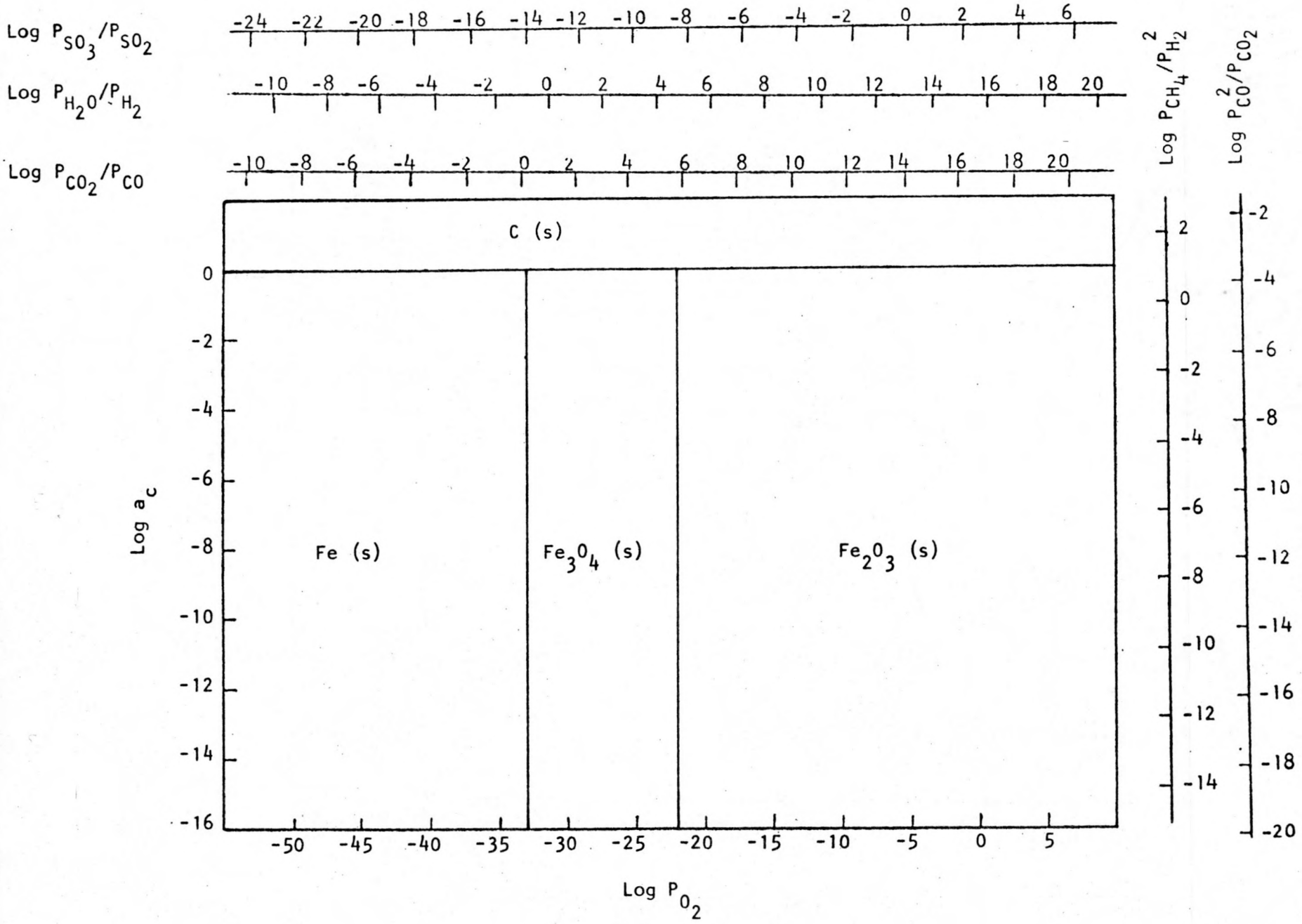

Fig. 32: Phase Stability Diagram: Fe-C-O at 800°F (700°K).

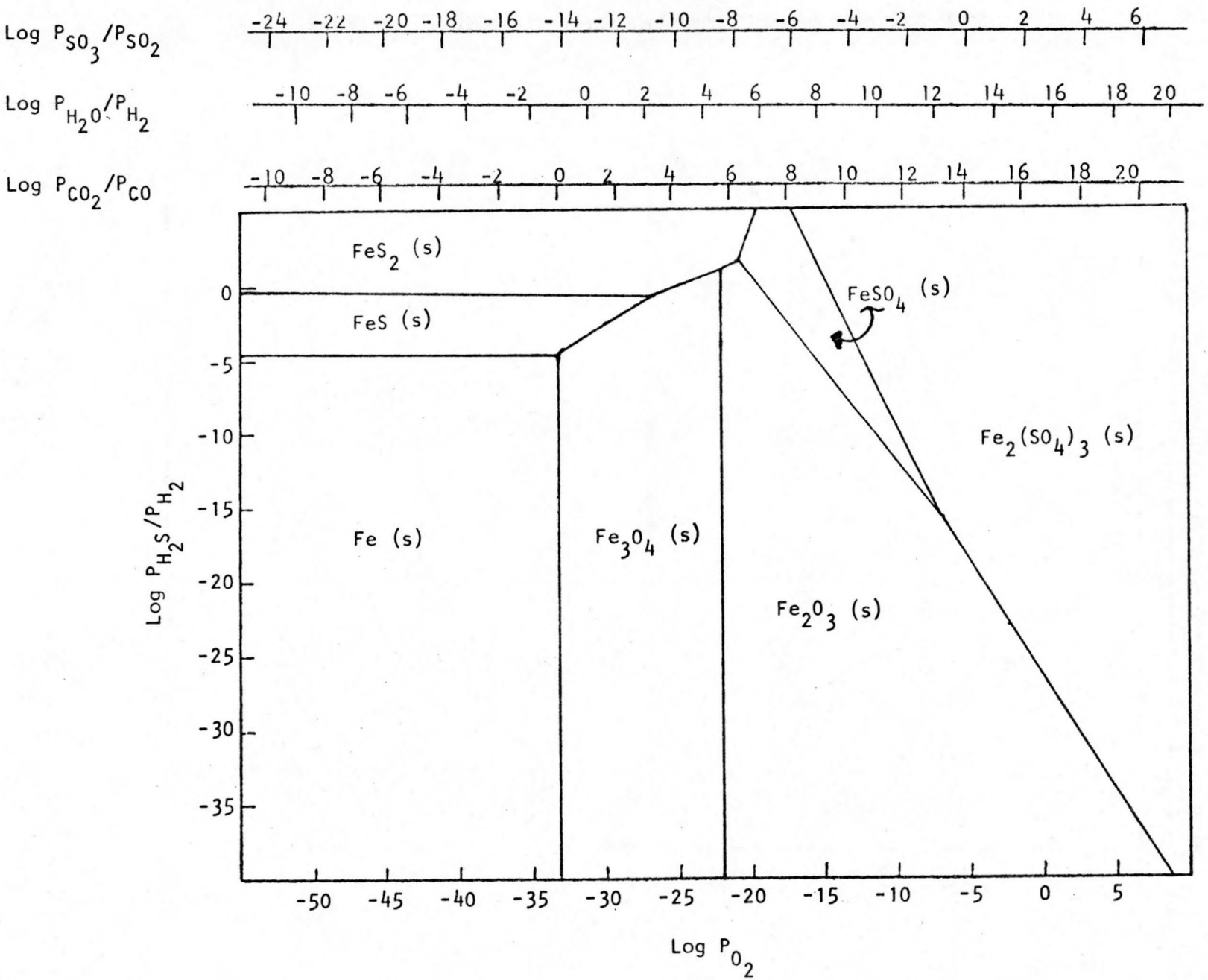

Fig. 33: Phase Stability Diagram: Fe-O-H_2S/H_2 at 800°F (700°K).

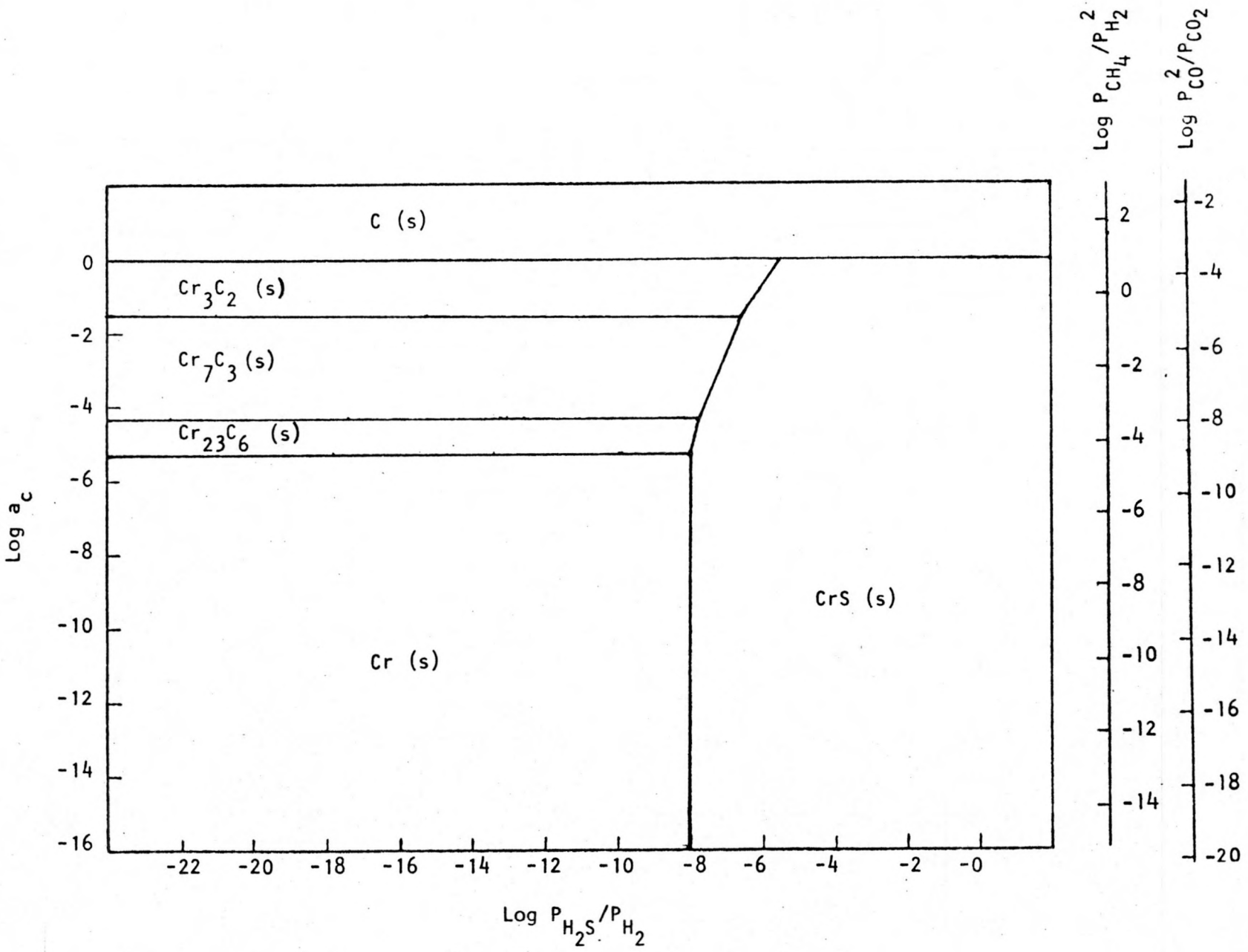

Fig. 34: Phase Stability Diagram: Cr-C-H_2S/H_2 at 800°F (700°K).

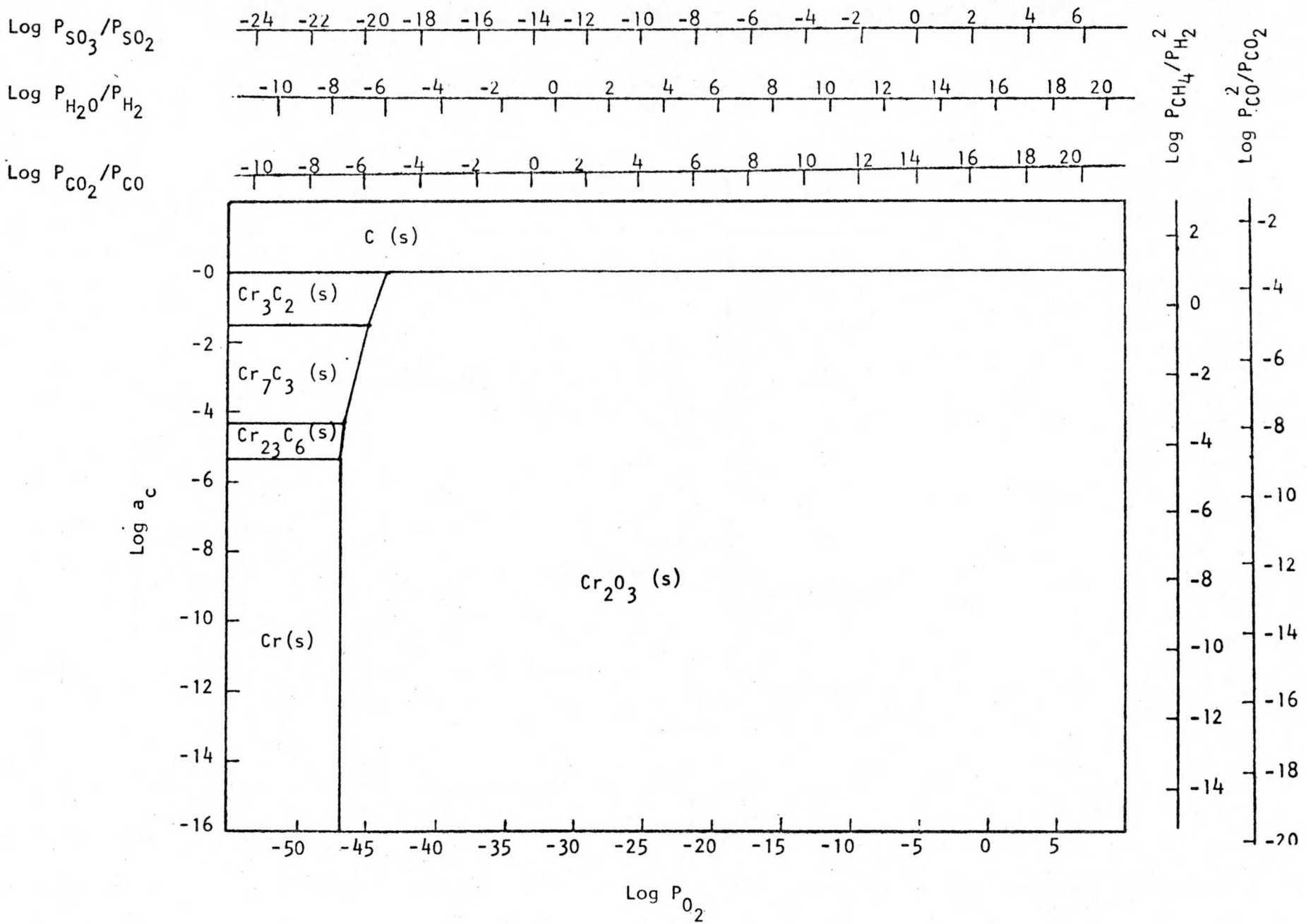

Fig. 35: Phase Stability Diagram: Cr-C-O at 800°F (700°K).

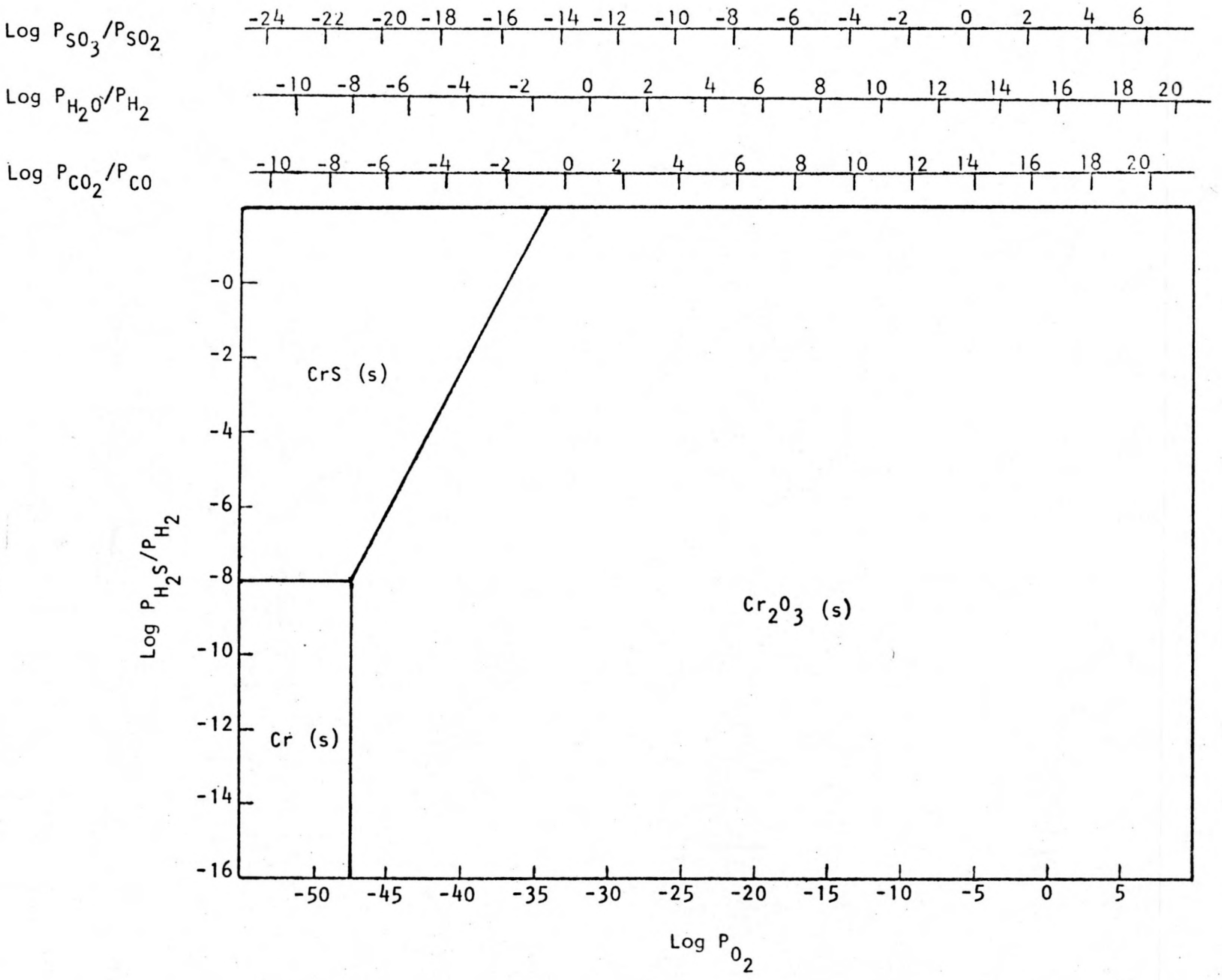

Fig. 36: Phase Stability Diagram: Cr-O-H_2S/H_2 at 800°F (700°K).

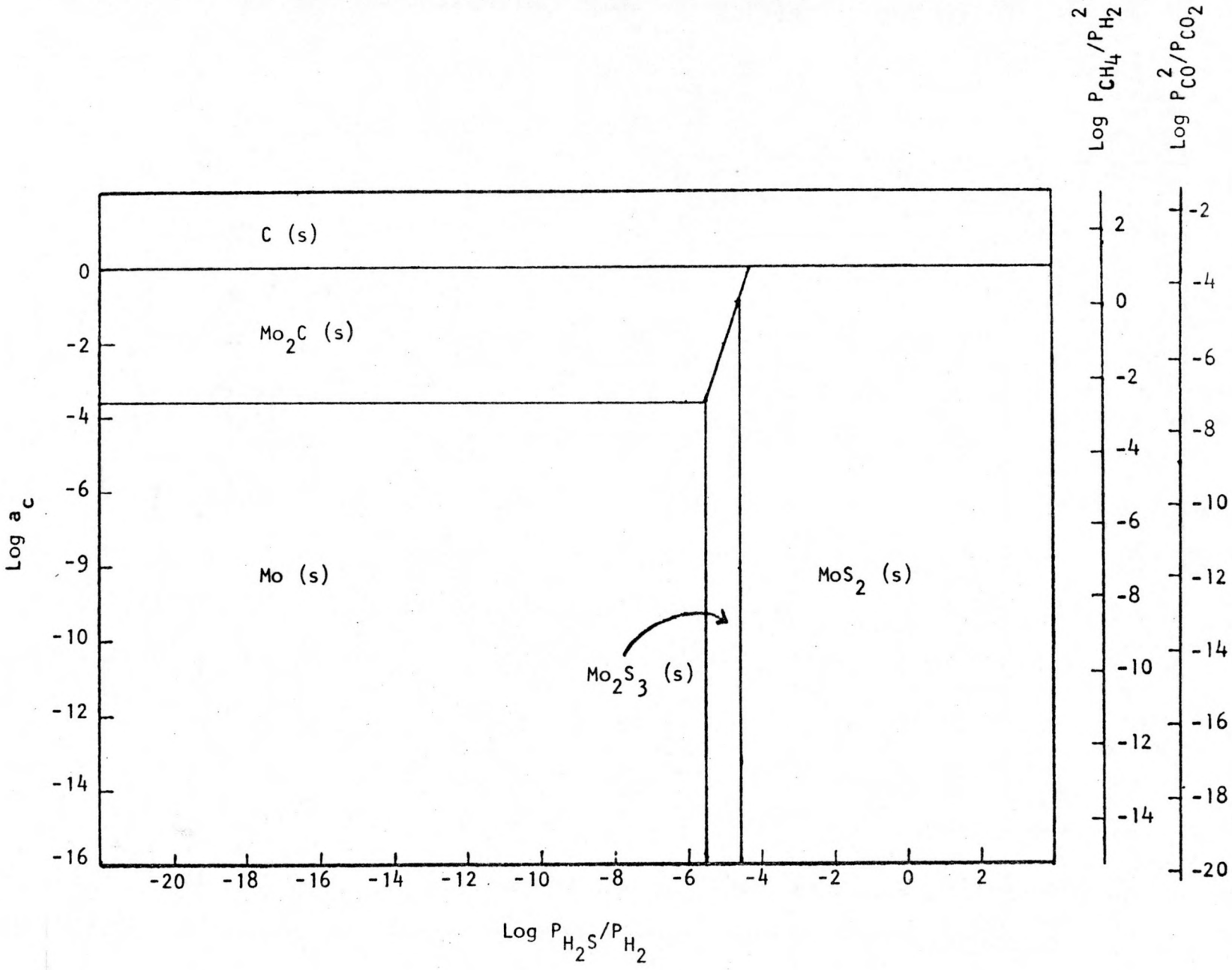

Fig. 37: Phase Stability Diagram: Mo-C-H_2S/H_2 at 800°F (700°K).

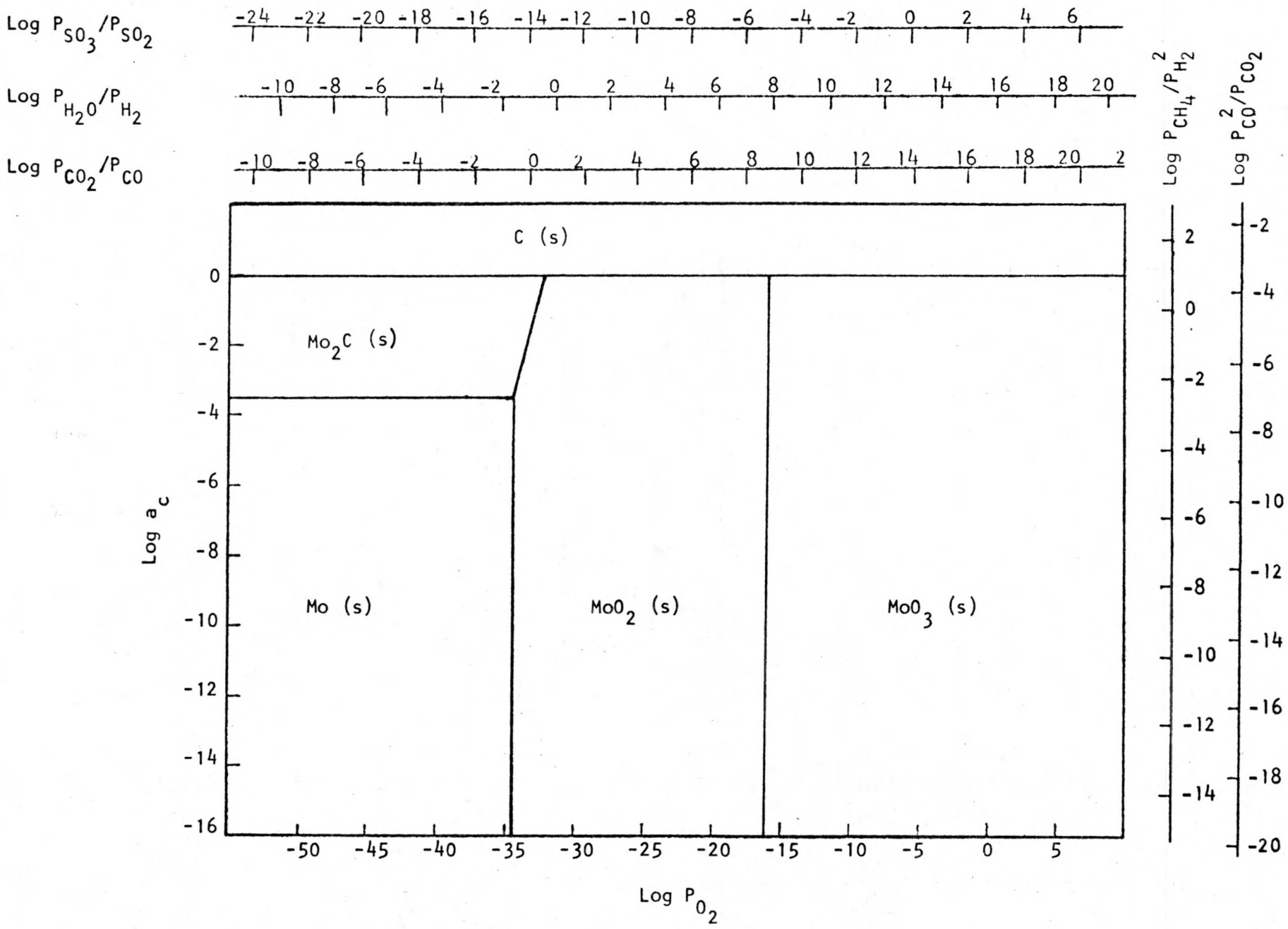

Fig. 38: Phase Stability Diagram: Mo-C-O at 800°F (700°K).

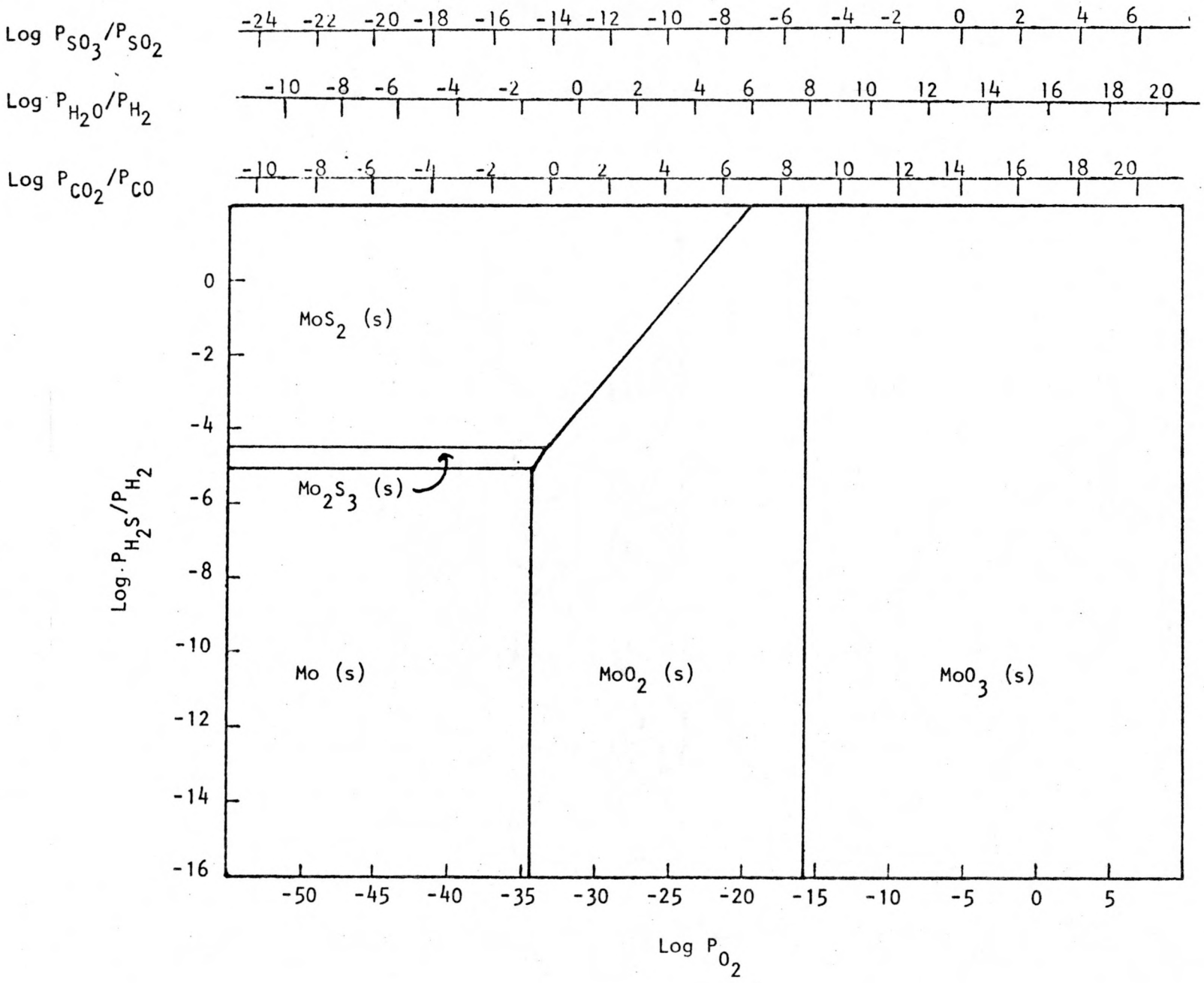

Fig. 39: Phase Stability Diagram: Mo-O-H_2S/H_2 at 800°F (700°K).

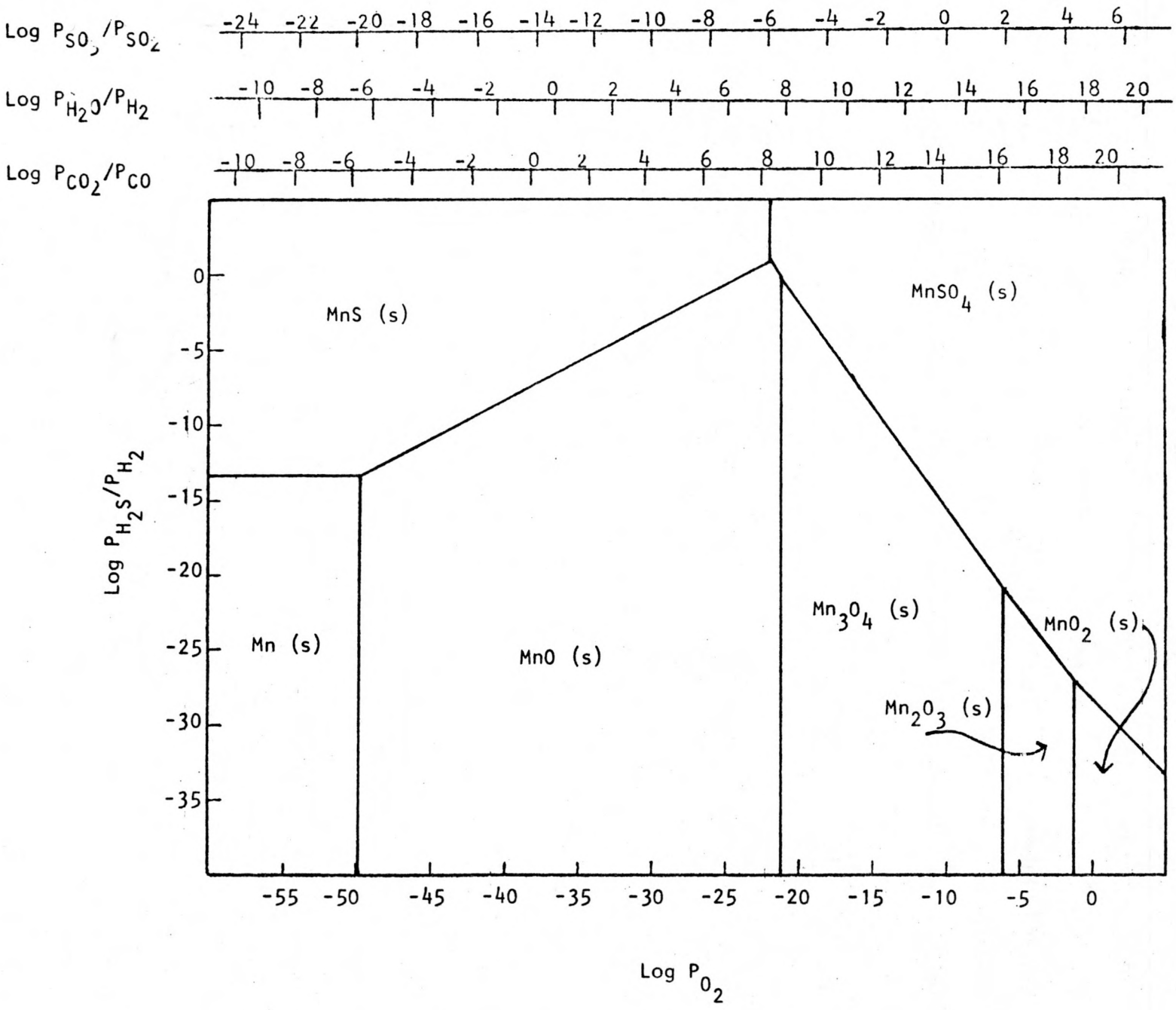

Fig. 40: Phase Stability Diagram: Mn-O-H_2S/H_2 at 800°F (700°K).

WORK FORECAST

Dynamic crack growth studies at high temperatures and pressures of argon, hydrogen and coal slurry gases are presently underway and should be completed for the next report. J_{IC} tests will be run at 800°F in hydrogen gas and slurry gases. Electron microprobe and X-Ray analyses of corrosion scales and condensates is partially done and should be completed for the next report. Hydrogen attack studies are continuing in order to establish the Nelson curve.

Distribution List for Technical Reports

Name and Address

S. J. Dapkunas (2)
Department of Energy
Div. of Planning and Systems
Engineering
Mail Stop C-156 (GTN)
Washington, DC 20545

R. A. Bradley, Manager (4)
Fossil Energy Materials Project
Oak Ridge National Laboratory
P. O. Box X
Oak Ridge, TN 37830

S. J. Schneider (2)
National Bureau of Standards
Department of Commerce
Washington, DC 20234

E. E. Hoffman, Chief (1)
Energy Materials and Systems Branch
Oak Ridge Operations Office
Department of Energy
P. O. Box E
Oak Ridge, TN 37830

Richard Schorr (1)
Battelle Columbus Lab
505 King Avenue
Columbus, OH 43201

R. P. Wei (1)
Lehigh University
Center for Surface and Coatings
Branch
Bethlehem, PA 18015

Dilip Bhandarkar (1)
Lawrence Berkeley Laboratory
University of California
Berkeley, CA 94720

D. Canonico (1)
Oak Ridge National Laboratory
P. O. Box X
Oak Ridge, TN 37830

Technical Information Center (245)
Department of Energy
Oak Ridge, TN 37830

J. Slaughter (1)
Oak Ridge National Laboratory
P. O. Box X
Oak Ridge, TN 37830

W. J. Lochmann (1)
The Ralph M. Parsons Co.
100 West Walnut Street
Pasadena, CA 91124

G. Sorell (1)
Exxon Research and Engineering Company
P. O. Box 101
Florham Park, NJ 07932

William E. Erwin (1)
Engineering Department
Standard Oil Company of California
P. O. Box 1272
Richmond, CA 94802

G. Catus (1)
109 Office & Laboratory
Ames Laboratory
Iowa State University
Ames, IA 50011

R. Fisher (2)
321 Spedding
Ames Laboratory
Iowa State University
Ames, IA 50011

T. Scott (5)
126 Metals Development Building
Ames Laboratory
Iowa State University
Ames, IA 50011

Charles M. Woods (10)
204 Metals Development Building
Ames Laboratory
Iowa State University
Ames, IA 50011

Burton Gleason (10)
201 Spedding
Ames Laboratory
Iowa State University
Ames, IA 50011